



HAL
open science

Experimental determination of the role of diffusion on Li isotope fractionation during basaltic glass weathering

A. Verney-Carron, Nathalie Vigier, Romain Millot

► To cite this version:

A. Verney-Carron, Nathalie Vigier, Romain Millot. Experimental determination of the role of diffusion on Li isotope fractionation during basaltic glass weathering. *Geochimica et Cosmochimica Acta*, 2011, 75, pp.3452-3468. 10.1016/j.gca.2011.03.019 . hal-00673515

HAL Id: hal-00673515

<https://brgm.hal.science/hal-00673515>

Submitted on 23 Feb 2012

HAL is a multi-disciplinary open access archive for the deposit and dissemination of scientific research documents, whether they are published or not. The documents may come from teaching and research institutions in France or abroad, or from public or private research centers.

L'archive ouverte pluridisciplinaire **HAL**, est destinée au dépôt et à la diffusion de documents scientifiques de niveau recherche, publiés ou non, émanant des établissements d'enseignement et de recherche français ou étrangers, des laboratoires publics ou privés.

Accepted Manuscript

Experimental determination of the role of diffusion on Li isotope fractionation during basaltic glass weathering

A. Verney-Carron, N. Vigier, R. Millot

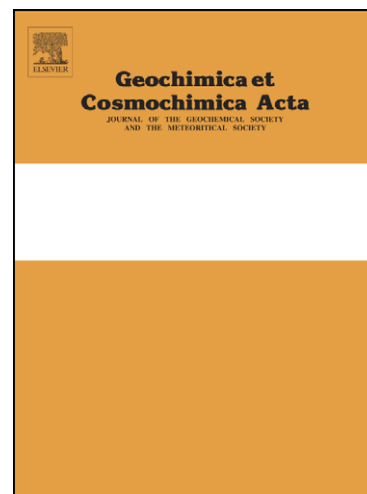
PII: S0016-7037(11)00175-X
DOI: [10.1016/j.gca.2011.03.019](https://doi.org/10.1016/j.gca.2011.03.019)
Reference: GCA 7148

To appear in: *Geochimica et Cosmochimica Acta*

Received Date: 19 July 2010
Accepted Date: 15 March 2011

Please cite this article as: Verney-Carron, A., Vigier, N., Millot, R., Experimental determination of the role of diffusion on Li isotope fractionation during basaltic glass weathering, *Geochimica et Cosmochimica Acta* (2011), doi: [10.1016/j.gca.2011.03.019](https://doi.org/10.1016/j.gca.2011.03.019)

This is a PDF file of an unedited manuscript that has been accepted for publication. As a service to our customers we are providing this early version of the manuscript. The manuscript will undergo copyediting, typesetting, and review of the resulting proof before it is published in its final form. Please note that during the production process errors may be discovered which could affect the content, and all legal disclaimers that apply to the journal pertain.



1 Experimental determination of the role of diffusion on Li isotope fractionation
2 during basaltic glass weathering

3

4

5 A. Verney-Carron ^{a,1*}, N. Vigier ^a, R. Millot ^b

6

7 ^a CRPG-CNRS, 15 rue Notre Dame des Pauvres, 54501 Vandoeuvre les Nancy, France

8 ^b BRGM, Metrology Monitoring Analysis Department, 3 avenue Claude Guillemin, BP 36009, 45060 Orléans

9 Cedex 2, France

10 ¹Present address: LISA, UMR 7583, UPEC, UPD, 61 avenue du Général de Gaulle, 94010 Créteil Cedex,

11 France.

12

13

14

15 Revised version 14 March 2011

16

17 Keywords: Li isotopes, isotope fractionation, diffusion, basaltic glass

18 **Abstract**

19

20 In order to use lithium isotopes as tracers of silicate weathering, it is of primary
21 importance to determine the processes responsible for Li isotope fractionation and to
22 constrain the isotope fractionation factors caused by each process as a function of
23 environmental parameters (e.g. temperature, pH). The aim of this study is to assess Li isotope
24 fractionation during the dissolution of basalt and particularly during leaching of Li into
25 solution by diffusion or ion exchange. To this end, we performed dissolution experiments on a
26 Li-enriched synthetic basaltic glass at low ratios of mineral surface area/volume of solution
27 (S/V), over short timescales, at various temperatures (50 and 90°C) and pH (3, 7, and 10).
28 Analyses of the Li isotope composition of the resulting solutions show that the leachates are
29 enriched in ${}^6\text{Li}$ ($\delta^7\text{Li} = +4.9$ to $+10.5\text{‰}$) compared to the fresh basaltic glass ($\delta^7\text{Li} = +10.3 \pm$
30 0.4‰). The $\delta^7\text{Li}$ value of the leachate is lower during the early stages of the leaching process,
31 increasing to values close to the fresh basaltic glass as leaching progresses. These low $\delta^7\text{Li}$
32 values can be explained in terms of diffusion-driven isotope fractionation. In order to quantify
33 the fractionation caused by diffusion, we have developed a model that couples Li diffusion
34 with dissolution of the glassy silicate network. This model calculates the ratio of the diffusion
35 coefficients of both isotopes ($a=D_7/D_6$), as well as its dependence on temperature, pH, and
36 S/V. a is mainly dependent on temperature, which can be explained by a small difference in
37 activation energy (0.10 ± 0.02 kJ/mol) between ${}^6\text{Li}^+$ and ${}^7\text{Li}^+$. This temperature dependence
38 reveals that Li isotope fractionation during diffusion is low at low temperatures ($T < 20^\circ\text{C}$),
39 but can be significant at high temperatures. However, concerning hydrothermal fluids ($T >$
40 120°C), the dissolution rate of basaltic glass is also high and masks the effects of diffusion.
41 These results indicate that the high $\delta^7\text{Li}$ values of river waters, in particular in basaltic

42 catchments, and the fractionated values of hydrothermal fluids are mainly controlled by
43 precipitation of secondary phases.

ACCEPTED MANUSCRIPT

44

1. INTRODUCTION

45

46 Silicate weathering has a major impact on the carbon cycle over long timescales,
47 because Ca and Mg are released during dissolution of silicate minerals which in turn leads to
48 consumption of atmospheric carbon dioxide via formation of carbonate in the oceans (e.g.
49 Ludwig et al., 1999; Dupré et al., 2003; Lerman et al., 2007; Franck et al., 2008; Hartmann et
50 al., 2009). Basalt are among the most easily weathered silicate rocks, therefore basalt
51 weathering potentially represents a significant atmospheric CO₂ sink and a major source of
52 oceanic Ca and Mg (Louvat and Allègre, 1997, 1998; Gaillardet et al., 1999; Dessert et al.,
53 2003). Assessing the contribution of basaltic weathering to rivers is therefore of primary
54 importance. A significant portion of basalt weathering is likely due to alteration of basaltic
55 glass: the glassy phase and hyaloclastites have been shown to play a key role in determining
56 the chemical and isotope compositions of river waters in volcanic regions (e.g. Gislason and
57 Oelkers, 2003, and references therein; Wolff-Boenisch et al., 2004; Vigier et al., 2006). This
58 is consistent with their more rapid dissolution relative to basalt minerals (e.g. Wolff-Boenisch
59 et al., 2006).

60 In this context, lithium isotopes could represent a powerful tracer of basalt weathering
61 as river Li isotope compositions appear to be correlated with weathering rates of silicate
62 lithologies present within the basin (Kisakürek et al., 2005; Vigier et al., 2009; Pogge von
63 Strandmann et al., 2010; Millot et al., 2010b). Lithium has two stable isotopes, ⁶Li and ⁷Li,
64 whose large relative mass difference is responsible for significant isotopic fractionation
65 during physico-chemical processes. Lithium is comparatively enriched in silicates (5 to 33
66 ppm for the continental crust, Teng et al, 2008) but is present at low concentrations in
67 carbonates (< 2 ppm, Hoefs and Sywall, 1997). Moreover, this element does not play a
68 significant role in biological or atmospheric cycles (Lemarchand et al., 2010; Millot et al.,

69 2010c). The Li isotope compositions of catchment rocks and river waters are significantly
70 different with rivers systematically enriched in ^7Li . To date, this has been interpreted as the
71 result of Li isotopic fractionation during silicate weathering (Huh et al., 1998, 2001; Pogge
72 von Strandmann et al., 2008, 2010; Vigier et al., 2009; Millot et al., 2010a). In more detail,
73 the ^7Li enrichment of dissolved loads of river waters has been explained by (1) the formation
74 of secondary phases, especially clay minerals, and their preferential uptake of ^6Li (e.g. Chan
75 and Edmond, 1988; Chan et al., 1992; Vigier et al., 2008) and (2) a preferential release of ^7Li
76 from the mineral into solution (Huh et al., 2004; Kısakürek et al., 2004; Rudnick et al., 2004;
77 Teng et al., 2004). This second assumption was supported by the particularly high $\delta^7\text{Li}$ values
78 ($\delta^7\text{Li} = ((^7\text{Li}/^6\text{Li})_{\text{sample}} / (^7\text{Li}/^6\text{Li})_{\text{LSVEC}} - 1) \times 1000$) measured in river waters draining areas
79 with little or no soils, such as the Canadian shield (Millot et al., 2010b) or high altitude zones
80 in the Andes and the Himalayas (Huh et al., 2001; Kısakürek et al., 2005).

81 Preferential uptake of ^6Li during the formation of clay minerals was initially suggested
82 by field studies (e.g. Chan and Edmond, 1988; Chan et al., 1992, 1994, 2002; Zhang et al.,
83 1998) and then confirmed by experimental work (e.g. Williams and Hervig, 2005; Vigier et
84 al., 2008; Pistiner and Henderson, 2003). In contrast, preferential release of ^7Li during
85 weathering of minerals has not been verified in the laboratory. Leaching experiments have
86 been performed with basalt, weathered basalt and sediments at high temperatures (up to
87 350°C) and pressures (400-800 bars) with the aim of assessing the contributions of basalt
88 and/or sediment leaching to the Li budget during alteration in hydrothermal systems (Chan et
89 al., 1994; Seyfried et al., 1998, James et al., 2003). These authors reported fluid $\delta^7\text{Li}$ values
90 initially heavier than those of the mineral but then progressively becoming lighter
91 (approaching that of the starting mineral). All these experiments were conducted under rock-
92 dominated conditions (i.e. high reactive surface area/volume of solution, S/V, or low
93 water/rock ratio, W/R). These conditions greatly favour the formation of secondary mineral

94 phases which could also influence the Li isotopic compositions measured in solution.
95 Experiments conducted by Millot et al. (2010a) were carried out at lower temperatures (25 to
96 250°C), but also at relatively low W/R ratio, with the intention of precipitating secondary
97 phases even at the onset of the experiment. Pistiner and Henderson (2003) performed basalt
98 alteration experiments at low pH (~ 1) and low S/V (to avoid precipitation of secondary
99 minerals), and did not observe any significant isotope fractionation after 1 week of
100 dissolution. Finally, recent forsterite and basalt glass dissolution experiments were conducted
101 by Wimpenny et al. (2010) at far from equilibrium conditions and at low pH and temperature.
102 The results revealed no isotope fractionation during leaching of forsterite. For the basalt glass
103 the $\delta^7\text{Li}$ values of the leachates produced by weathering are equal or slightly lower than the
104 fresh glass $\delta^7\text{Li}$ value.

105 In this study, we performed leaching experiments on basaltic glass at far from
106 equilibrium conditions in order to favour leaching/dissolution processes, and to minimise any
107 potential secondary mineral precipitation. The objective is to quantify Li isotopic
108 fractionation during the leaching/dissolution process. To this end, the experiments were
109 conducted at very low S/V ratios (i.e. very high water/rock ratio). The basaltic glass was
110 highly enriched in lithium in order to permit precise measurements of Li isotope in the
111 leachates during the early stages of the alteration process. By combining major element and
112 Li isotope data, we have developed a coupled diffusion-dissolution model which quantifies Li
113 isotope fractionation.

114

115 **2. EXPERIMENTAL METHODS AND ANALYTICAL PROCEDURES**

116

117 **2.1. Experimental setup**

118

119 *2.1.1. Materials*

120 A synthetic basaltic glass was doped with 1% Li₂O using the procedure described in
121 Techer et al. (2001), i.e. by melting a mixture of powdered oxides, carbonates, nitrates and
122 phosphates in alumina crucibles for 3 h at 1500°C. The resulting melt was then poured into
123 graphite crucibles preheated at 700°C. The glass was heat treated at 670°C for 1 h, then
124 cooled to room temperature in 10 h. Concentrations of major cations (Si, Al, Fe, Mn, Mg, Ca,
125 Na K, Ti, and P) were determined by ICP-AES (IRIS Thermo Elemental) at the SARM
126 (French national facilities, Nancy). Li concentrations were analyzed using atomic absorption
127 spectrometry (AAS) (VARIAN220 FS) at the SARM. Uncertainties range between 5 and 20%
128 depending on the element and its concentration.

129 The homogeneity of Li isotopic composition of the glass was determined by ion
130 microprobe (CAMECA ims3f), using classical energy filtering techniques (Chaussidon and
131 Robert, 1998). The samples were sputtered with a 3nA primary O⁻ beam then secondary
132 positive ions including ⁶Li⁺ and ⁷Li⁺ were accelerated at 4.5 kV and were analysed at a mass
133 resolution M/ΔM of 1200 (to remove the interfering ⁶LiH⁺ at mass 7) and with the energy slit
134 centred and fully opened. Counting times were 9s for ⁶Li and 3s for ⁷Li over 40 cycles.

135

136 *2.1.2. Reactive surface area determination*

137 The synthetic basaltic glass was ground and sieved in order to recover the 40-100 μm
138 particle size fraction which was then washed and ultrasonicated in acetone in order to remove
139 any finer particles remaining. The glass powder was stirred in a beaker containing 12 cm
140 depth of acetone. According to Stokes' law, >40 μm particles reach the bottom of the beaker
141 in 15 s; after this time, the supernatant solution is removed from the beaker. This procedure
142 was repeated until the supernatant was clear. The specific surface area was measured by
143 krypton adsorption using the BET method and is 842 ± 5 cm² g⁻¹. To assess the consistency of

144 this result, the BET value was compared with the geometric surface area (in $\text{cm}^2 \text{g}^{-1}$) which
 145 can be expressed as the product of the surface area of a sphere (S_{sphere}) by the number of
 146 spheres (n) divided by the mass (m) of the n spheres:

147

$$148 \quad S_{\text{geo}} = \frac{n \times S_{\text{sphere}}}{m} = \frac{n \times 4\pi r^2}{n \times \frac{4}{3}\pi r^3 \times \rho} = \frac{3}{\rho \times r} \quad (1)$$

149

150 where ρ is the density of the glass ($2.7 \pm 0.1 \text{ g cm}^{-3}$, measured by pycnometry) and r is the
 151 grain average radius (in cm). While Eq. (1) yields a geometric surface area of $350 \text{ cm}^2 \text{g}^{-1}$ that
 152 is 2.4 times lower than the measured surface area these results are nevertheless consistent
 153 because surface roughness and the non-spherical nature of the grains will increase true surface
 154 area compared to that calculated by Eq. (1).

155

156 2.1.3. Experiments

157 The objective of the experiments (PW-90, PH3-90, PH10-90, and PW-50; Table 1)
 158 was to determine the evolution of Li concentration and isotopic composition of the leachate at
 159 'far from equilibrium' conditions. For this, these experiments were carried out in Savillex®
 160 PTFE reactors under static conditions, at a low S/V ratio (0.7 cm^{-1}) and over short timescales
 161 (< 4 days). The batch solution was not stirred in order to prevent grinding of the glass and
 162 progressive increase of the reactive surface area. However, the mass of glass introduced in the
 163 reactor is sufficiently low (~ 50 mg for the majority of experiments) so that transport processes
 164 are never rate-limiting.

165 For the experiments performed in pure water (Milli-Q water) (PW) at 90 and 50°C
 166 (PW-90 and PW-50), a separate reactor was used for each run. Typically, 50 mg of glass
 167 powder was placed in the Savillex® PTFE reactors with 50 mL of solution. For the other

168 experiments, one single larger reactor (120 or 250 mL) was used. Each time the solution was
169 sampled, the reactor was manually agitated and opened for a maximum of a few minutes.

170 The pH was measured at the in situ temperature. However, the temperature of the
171 sampled aliquot can rapidly decrease during pH measurements. Consequently, the
172 temperature was also monitored during the pH measurement for calculations. The samples
173 were filtered at 0.45 μm , and then acidified with concentrated HNO_3 to obtain 0.3 N HNO_3
174 for ICP-AES and AAS analyses.

175 Both the influence of pH (pure water, pH 3 and pH 8.4 at 90°C) and temperature (50
176 and 90°C) were tested. An initial pH of 3 was obtained by addition of 0.001 M HCl, and an
177 initial pH of 8.4 at 90°C was obtained by addition of 0.0001 M NaOH. In order to determine
178 the influence of the S/V ratio, two leaching experiments were carried out with pure water at
179 90°C, with a S/V ratio of 0.7 and 7 cm^{-1} respectively, simply by changing the amount of glass
180 powder initially introduced into the beaker (experiments SV1 and SV2, respectively, see
181 Table 1).

182

183 2.2. Li isotope analyses

184

185 In order to analyse the Li isotopic composition of the synthetic basaltic glass, the
186 complete dissolution of ~ 10 mg of glass was performed using a mixture of concentrated
187 hydrofluoric and nitric acids heated on a hotplate at 100°C, in a closed Teflon beaker for 1
188 day. The solutions were then evaporated, re-dissolved in 1M HCl, and ultrasonicated.

189 For analysis of the leachate samples, an aliquot containing 30 - 60 ng of Li was
190 evaporated and re-dissolved in 1 M HCl.

191 Li was separated from the sample matrix by cation exchange chromatography, as
192 described in Vigier et al. (2008) and Lemarchand et al. (2010). Li isotopes were measured on

193 pure Li fractions with a Thermo-Fisher Neptune Multi Collector-ICP-MS at the BRGM
194 (Orléans, France) (Millot et al., 2004), and with a Nu Instruments Multi Collector-ICP-MS at
195 the ENS (Lyon, France). Li isotope ratios were measured relative to the L-SVEC standard
196 solution (NIST SRM 8545, Flesch et al., 1973) using a standard-sample bracketing technique
197 in order to correct for instrumental mass bias. Li isotope ratios are expressed in δ notation as
198 the part per thousand (‰) deviation from L-SVEC composition.

199 For MC-ICP-MS measurements with the Neptune (BRGM), the analytical protocol
200 involved acquisition of 15 ratios with 16 s integration time per ratio, and yielded in-run
201 precision better than 0.2‰ (2σ). Blank values were low (i.e. 0.2‰ of the Li signal) and 5
202 minutes wash time was sufficient to reach a stable background value. The Li concentration in
203 solution required for analysis was 30 ppb. The accuracy and reproducibility of the whole
204 method (separation + MC-ICP-MS analysis) was tested by repeated measurements of a
205 seawater standard solution (IRMM BCR-403, Millot et al., 2004) and the Li7-N reference
206 solution (Carignan et al., 2007) (Table 2).

207 The Li isotopic compositions we determined for Li7-N and seawater BCR-403 were
208 $+30.8 \pm 0.5$ ‰ ($n = 10$) and $+31.3 \pm 0.4$ ‰ ($n = 10$), respectively, which are in agreement
209 with published values (Millot et al., 2004; Carignan et al., 2007 and references therein). The
210 accuracy and reproducibility of the MC-ICP-MS analysis (without separation chemistry) was
211 also assessed during the session with two standards, Li7-N and Li-6N (Carignan et al., 2007).
212 The average values are $\delta^7\text{Li} = +30.3 \pm 0.2$ ‰ ($n = 10$) for Li7-N and $\delta^7\text{Li} = -8.1 \pm 0.3$ ‰ ($n =$
213 10) for Li6-N, and are similar to values reported in the literature (Carignan et al., 2007).

214 For both sessions of MC-ICP-MS measurements with the Nu Instruments (ENS-
215 Lyon), the typical Li concentration of the analysed solutions was 60 ppb. The accuracy and
216 reproducibility of the method was tested with the JB-2 basalt standard (Table 2). The $\delta^7\text{Li}$
217 value of JB-2 is $+4.0 \pm 0.3$ ‰ ($n = 1$) which is consistent with published values (e.g. Carignan

218 et al., 2007). The values of the three standards, SW BCR403, Li7-N, and Li6-N, are also in
219 agreement with previously reported values (Table 2). Reference solutions were also analysed
220 at reduced concentrations in order to assess the reproducibility and the confidence in
221 measuring lower concentration solutions (Table 2). The $\delta^7\text{Li}$ of SW BCR403 at 15 ppb is
222 $+30.5 \pm 0.7 \text{ ‰}$ ($n = 2$). The $\delta^7\text{Li}$ of Li7-N (10 to 40 ppb) does not change significantly as a
223 function of Li content. However, the corresponding internal errors are higher when the Li
224 concentrations are lower (see Table 2).

225

226 **2.3. Calculation of solution saturation states**

227

228 Analyses of the chemical composition and temperature measurements of the leachate
229 solutions can be used to calculate mineral saturation indices using the JCHESS speciation
230 code (van der Lee and De Windt, 2002). JCHESS uses a thermodynamic database which is
231 based on the EQ3/6 database (Wolery, 1992). Because of the rapid cooling (around 75°C) of
232 the solution during the pH measurements, the solution pH was recalculated from the major
233 cation concentrations, by assuming electroneutrality at the measurement temperature. If the
234 agreement between the measured pH and the calculated value is good, then both the solution
235 analyses and the pH measurements are valid. The solution pH at the temperature of the
236 experiment (90 or 50°C) was recalculated by changing the temperature in JCHESS.

237

238

3. RESULTS

239

240 **3.1. Composition of the fresh synthetic basaltic glass**

241

242 The composition of the synthetic basaltic glass is given in Table 3. Its composition is
243 consistent with published analyses for the same glass (Techer et al., 2001). Except for the
244 enrichment in Li, the composition is typical of basalt from mid-ocean ridges (MORB) (e.g.
245 Schiano et al., 1997).

246 The bulk Li isotopic composition of the fresh synthetic basaltic glass was determined
247 for 3 different powder aliquots by MC-ICP-MS and is $+10.3 \pm 0.4 \text{ ‰}$ (2σ). The homogeneity
248 of the glass Li isotopic composition was also determined by ion microprobe. The standard
249 deviation of 34 measurements in 2 different grains is 0.7‰ . The standard deviation of the
250 GB4 glass standard (Chaussidon and Robert, 1998) analysed during the same session is 0.4‰
251 ($n=7$). The synthetic basaltic glass used for the alteration experiments is therefore considered
252 to be isotopically homogeneous, relative to the overall uncertainty of the Li isotope
253 measurements.

254

255 **3.2. pH and chemical composition of the leachates**

256

257 At 90°C , the agreement between measured and calculated pH (from major elements)
258 was good. For example, the pH measured at 75°C for the PH10-90 experiment after 1 day was
259 8.5. The pH calculated from elemental concentrations in solution is also 8.5 at 75°C . Thus the
260 pH recalculated at the temperature of the experiment, i.e. 90°C , is 8.3 (see Table 4). For this
261 experiment the difference between experimental and calculated pH at the measurement
262 temperature is never higher than 0.1 pH unit. For the other experiments, the difference is
263 always less than 0.3 pH unit, except for the fluid sampled towards the end of the experiments
264 (34 d for pH3-90, 63 d for experiments SV1 and SV2) where the discrepancy reaches 0.7 pH
265 unit, probably because of carbonation effects that decrease the measured pH.

266 For experiments performed in pure water at 90°C (PW-90, SV1, SV2), the pH rapidly
267 increases to 8.5-9. For the experiment PH10-90, the initial pH of 8.4 remains more or less
268 constant. In the experiments with dilute nitric acid, the pH starts at a value of 3 and then does
269 not evolve significantly, except at 34 days. In the experiment performed at 50°C, pH increases
270 from 6.6 to 7.7 (Table 4).

271 The evolution of the silicon concentration in solution (Table 4, Fig. 1a) is quite similar
272 for all of the experiments performed at 90°C. The Si content increases linearly as a function
273 of time, as expected by a pure and constant dissolution process, and then reaches a plateau at
274 around 15-18 mg L⁻¹ after a few days. It is noteworthy that lithium concentration is not a
275 linear function of time, and the pattern is different for different experiments (Table 4, Fig 1b).
276 Solution lithium contents are lower for experiments at S/V=0.7 cm⁻¹ than they are for
277 experiments with S/V = 7 cm⁻¹.

278 In order to compare the behaviour of all the analysed elements in more detail,
279 concentrations can be converted to the normalized mass loss ($NL(i)$). $NL(i)$ corresponds to the
280 concentration C_i in solution (where i is the element analyzed) in g L⁻¹ corrected for the S/V
281 ratio and the initial glass mass fraction. $NL(i)$ is expressed in g m⁻² and is given by:

282

$$283 \quad NL(i) = \frac{C_i \times V}{S \times x_i} \quad (2)$$

284

285 where x_i is the initial fraction of the element i in the bulk glass.

286 $NL(i)$ therefore represents the equivalent quantity of leached glass per unit area.
287 Consequently, the NL notation allows a direct comparison of each element (i) released into
288 solution for all the experiments. Indeed, if the NL values are equal for all elements, then
289 dissolution can be considered to be congruent. In contrast, if the NL value of a particular
290 element is higher or lower than the NL values for silicon, then the element is probably

291 affected by processes in addition to dissolution, such as diffusion or secondary phase
292 formation.

293 The NL values based on all the elements analysed in this study are reported in Table 5.
294 For the experiment PW-90, Al, Ca, and Mg releases are congruent with Si release, as they all
295 display similar NL values (Fig. 2). Ca and Mg are modifier cations in silicate network,
296 whereas Al and Si are network-forming cations. However, under the experimental conditions
297 used in this study, their behaviour is similar, indicating negligible formation of secondary
298 minerals. The alkalis (Na and Li) are mobile elements and their rates of release are greater
299 than Si, as NL values for Na and Li are systematically higher (Table 5). Their behaviour is
300 clearly non-stoichiometric. All the experiments display this discrepancy ($NL(Li,Na) >$
301 $NL(Si)$), except for the experiment at pH 3, where the dissolution is nearly congruent for
302 alkalis as well.

303

304 **3.3. Alteration kinetics of the basaltic glass**

305

306 The release of Si into solution is caused by hydrolysis of the glass network (Bunker,
307 1994; Oelkers, 2001). The dissolution rate intrinsically depends on the properties of the glass
308 (composition, structure, etc.), but also on the chemistry of the solution. Two kinetic regimes
309 can be distinguished: (1) The 'initial' or 'forward' dissolution rate is measured if the solution is
310 sufficiently renewed or diluted. Under these conditions, the evolution of Si concentrations in
311 solution (and therefore $NL(Si)$) is linear as a function of time, as observed in the first few
312 hours of the experiments (Fig. 2). (2) The dissolution rate drops as the solution chemical
313 composition approaches equilibrium (e.g. Aagard and Helgeson, 1982), and a gel layer forms
314 at the surface of the glass (e.g. Frugier et al., 2008). The accumulation of elements in solution,
315 especially silicon, decreases the dissolution rate, as it reduces the chemical affinity between

316 the solution and the glass. This chemical affinity term is a parameter often used in kinetic
317 laws describing glass alteration (Grambow, 1985; Berger et al., 1994; Daux et al., 1997;
318 Frugier et al., 2009; Verney-Carron et al., 2010). The release of dissolved elements in solution
319 may also lead to the formation of secondary minerals. If this is the case, the dissolution
320 becomes incongruent.

321

322 3.3.1. Glass dissolution rate

323 For the experiment in pure water at 90°C (PW-90), the evolution of NL(Si) as a
324 function of time is constant between 0 and 0.6 days (Fig. 2). For the experiment in pure water
325 at 50°C (PW-50), the Si release rate is constant for the whole duration of the experiment (2
326 days). In both cases, the corresponding initial dissolution rate (r_0) normalized to the Si content
327 can be determined by linear regression of the data (Fig. 3a):

328

$$329 \quad r_0 = \frac{dNL(Si)}{dt} \quad (3)$$

330

331 The 'initial' dissolution rate r_0 is thus estimated to be 0.927 g/m²/d, i.e. 3.8×10^{-7} mol Si/m²/s
332 at 90°C and pH 8.6, and 0.0062 g/m²/d, i.e. 2.6×10^{-9} mol Si/m²/s at 50°C and pH 6.6 (Fig.
333 3a). These values are consistent with published data obtained at similar pH and temperatures
334 although it should be noted that there are large differences among basaltic glass dissolution
335 rate estimates reported in the literature (mainly caused by difficulties assessing the reactive
336 surface area). Initial dissolution rates for basaltic glass at pH between 8.2 and 8.6, and at
337 temperatures between 90°C and 100°C, range between 1.1×10^{-8} and 9.8×10^{-7} mol Si/m²/s
338 (Guy and Schott, 1989; Daux et al., 1997; Techer et al., 2000; Gislason and Oelkers, 2003).
339 At 50°C, the initial rate at neutral pH ranges between 2.1×10^{-10} and 1.9×10^{-8} mol Si/m²/s
340 (Guy and Schott, 1989; Gislason and Oelkers, 2003).

341 For the experiment in pure water at 90°C (PW-90), the Si release rate slows down after
342 0.6 days (Fig. 2). The corresponding dissolution rate calculated by linear regression is 0.08
343 $\text{g m}^{-2} \text{d}^{-1}$ between 0.6 and 4 days, i.e. one order of magnitude lower than the initial dissolution
344 rate (r_0). A similar feature is observed for the other experiments after a few hours (Table 4).
345 This highlights the feedback effect of the solution chemistry, especially dissolved silicon, on
346 glass dissolution kinetics (Aagard and Helgeson, 1982). For longer times (> 15 days), in
347 experiments SV1, SV2, pH3-90, and pH10-90, Si concentrations reach a plateau, which is
348 around 15-18 mg L^{-1} for experiments performed at 90°C. This plateau was also observed by
349 Techer et al. (2001) under similar conditions (pure water, 90°C, $S/V = 0.5 \text{ cm}^{-1}$) and likely
350 corresponds to a saturation state of the solution, i.e. to a decrease of the chemical affinity
351 term, and to secondary phase precipitation. The solution is still thermodynamically
352 undersaturated relative to silica phases, but is close to the solubility product of quartz (i.e. 19
353 mg L^{-1} at 90°C and $\text{pH} < 9.2$).

354 As discussed previously, the formation of secondary phases can be assessed by
355 comparing the normalized mass losses (NL). Iron forms oxides or hydroxides, whose
356 solubilities are very low, and $\text{NL}(\text{Fe})$ is much lower than $\text{NL}(\text{Si})$. Generally, Si, Al, Mg, and
357 Ca are able to be incorporated into secondary minerals, especially smectites, which are
358 frequently associated with basaltic glass alteration at these temperatures (Stroncik and
359 Schmincke, 2001; Crovisier et al., 2003). However, the relative difference between NL for
360 Ca, Al, Mg, and Si in all the experiments performed in this study is never more than 25%,
361 which is close to analytical uncertainties. Solution saturation indices have been calculated
362 using JCHESS in order to assess the potential formation of secondary minerals. In solutions
363 where Al concentrations were below detection limits, the leachates are undersaturated relative
364 to all the minerals of the database. The leachates where Al concentrations could be measured
365 are over-saturated relative to Al (oxi-)hydroxides (boehmite, diaspore, gibbsite), kaolinite

366 (rarely observed as an alteration product of the basaltic glass), and smectites for the
 367 experiments at alkaline pH (pH10-90). It is therefore possible that smectites formed during
 368 our experiments but in insufficient quantity to significantly affect the congruency of the
 369 dissolution, or to be observed by SEM.

370

371 3.3.2. *Li apparent diffusion coefficients*

372 The behaviour of the alkalis is non-stoichiometric for the first leaching steps of most
 373 experiments: the release rate of these elements is higher than that of Si, as witnessed by their
 374 greater normalized mass losses. This strongly suggests that the alkalis are controlled by a
 375 diffusion process, while Si is mainly controlled by dissolution at this stage of the experiment
 376 (as demonstrated by its initial linear evolution through time). Moreover, the Li normalized
 377 mass losses follows a square root time evolution, (Fig. 3b), as predicted by Fick's second law
 378 which predicts how diffusion causes concentration changes with time:

379

$$380 \left(\frac{\partial C}{\partial t} \right) = D \left(\frac{\partial^2 C}{\partial x^2} \right) \quad (4)$$

381

382 where the coordinate x is zero at the original glass surface, and where $C = 0$ at $x = 0$.

383 The resolution of this law can therefore be used to determine the apparent diffusion
 384 coefficient D_{app} of glass alkalis into solution from their concentrations in solution (e.g. Chave
 385 et al., 2007). For lithium, resolution of Eq. (4) leads to:

386

$$387 E_{HG} = \frac{NL(Li)}{\rho} = 2\sqrt{\frac{D_{app}t}{\pi}} \quad (5)$$

388

389 where E_{HG} is the equivalent hydrated glass thickness over which diffusion occurs, $NL(Li)$ the
390 normalized mass loss for lithium, ρ the glass density ($\rho = 2.7 \text{ g cm}^{-3}$). The D_{app} values can be
391 calculated by linear regressions ($NL(Li) = f(\sqrt{t})$). The slope corresponds to $2\rho\sqrt{(D_{app}/\pi)}$. The
392 calculated apparent diffusion coefficients for Li are $6.0 \times 10^{-19} \text{ m}^2 \text{ s}^{-1}$ at 90°C and pH 9, and
393 $3.5 \times 10^{-21} \text{ m}^2 \text{ s}^{-1}$ at 50°C and pH 6.6 (Fig. 3b).

394

395 **3.4. Respective contribution of the diffusion and dissolution processes**

396

397 In the early stages of the alteration process, Si is a tracer of dissolution while Li is
398 affected by diffusion and by dissolution. Consequently, the solution Si/Li ratio gives an
399 indication of the respective contribution of both processes (Table 4). Si/Li (%wt ratio) of the
400 fresh basaltic glass is 51. For all the experiments, the Si/Li ratios of the leachates are much
401 lower in the early stages of alteration (between 5 and 40, Table 4). This highlights Li
402 diffusion through the leached layer. The lowest Si/Li ratios (between 5 and 10) are found for
403 the experiment performed at 50°C , suggesting that the relative role of diffusion (compared to
404 dissolution) is greater at low temperature. This implies that the activation energy of the
405 diffusion process is lower than the activation energy of the dissolution process. For
406 experiments SV1 and SV2, characterized by different initial S/V, Si/Li ratios measured in the
407 leachates are significantly different, with Si/Li being 1.5 times lower for the high S/V ratio
408 experiment (SV2). With a greater reactive surface area, the silicon concentration of the
409 solution remains the same at saturation, but Li contents are significantly higher. This, again,
410 suggests that diffusion, which is a surface dependent process, partly controls the release of Li.

411

412 **3.5. Li isotopic composition of the leachates**

413

414 All the $\delta^7\text{Li}$ values of the leachates are equal to or lower than the $\delta^7\text{Li}$ of the fresh
415 basaltic glass (Fig. 4, Table 4), ranging between $+4.9 \pm 0.2 \text{ ‰}$ and $+10.5 \pm 0.2 \text{ ‰}$. The
416 amount of Li released in solution is always low compared to the amount of the Li available in
417 the glass: generally less than 10%, and less than 5% in the early stages of alteration. The
418 lowest solution $\delta^7\text{Li}$ values are found during the early stages of alteration. Then for
419 experiments PW-90, PH10-90 and SV1, $\delta^7\text{Li}$ increases with time to a plateau which is close to
420 the $\delta^7\text{Li}$ value of the fresh basaltic glass (Fig. 4). However, at a given temperature (90°C), the
421 $\delta^7\text{Li}$ value of the plateau is "lower" at high S/V ($+9.6 \pm 0.2 \text{ ‰}$ for experiment SV2) (Fig. 4c).

422 For a given S/V, $\delta^7\text{Li}$ evolves towards the fresh basaltic glass value more slowly at
423 50°C (PW-50) than at 90°C (PW-90) (Fig. 4a). After two days of leaching, $\delta^7\text{Li}$ is around
424 $+7.5 \pm 0.4 \text{ ‰}$ for the experiment performed at 50°C, whereas the fresh basaltic glass $\delta^7\text{Li}$
425 value is reached after less than 1 day for the 90°C experiments.

426 Comparison between the 90°C experiments performed at variable pH shows that at pH
427 3, the leachate $\delta^7\text{Li}$ remains lower than the fresh glass value for a longer time (up to 34 days).
428 In contrast, at high pH, $\delta^7\text{Li}$ rapidly reaches the fresh basaltic glass value (after a few hours)
429 and then remains constant, within uncertainties (Fig. 4b).

430 Wimpenny et al. (2010) performed experimental leaching of a natural basaltic glass at
431 far-from-equilibrium conditions in mixed through-flow reactors (open system). The $\delta^7\text{Li}$
432 values of the leachates in their experiments are also generally slightly lower than the mean
433 $\delta^7\text{Li}$ value of the pristine basaltic glass. Si/Li of the solutions, when analyzed, are also lower
434 than the mean basaltic glass value, at temperatures ranging between 25 and 45°C (the
435 temperature was varied during the experiment), suggesting a role of diffusion on the release
436 of Li into solution at these conditions.

437

438

4. DISCUSSION

439

440 **4.1. A coupled diffusion-dissolution model**

441

442 The low $\delta^7\text{Li}$ values relative to the fresh basaltic glass measured in the solutions
443 collected in the early stages of alteration strongly suggest that diffusion affects the Li isotope
444 signature of these solutions. Indeed, diffusion is expected to result in light isotope (^6Li)
445 enrichment in the solution relative to the solid phase. The role of diffusion on the Li isotope
446 signature at the beginning of the experiments is also supported by the fact that the lowest $\delta^7\text{Li}$
447 values also correspond to the lowest Si/Li (Table 4, section 3.4).

448 In order to quantify diffusion coefficients for ^6Li and ^7Li , we have developed a model
449 that takes into account both processes: release of Li by diffusion and release of Li by
450 dissolution of the glass network (Fig. 5). During alteration, glass network modifier cations,
451 such as alkali metals (Na^+ , Li^+), are replaced by hydrogen species (H_3O^+ , H_2O) present in
452 solution. This leads to a selective leaching of these metals, and to the formation of a "leached
453 layer" at the glass surface (Rana and Douglas, 1961a,b; Hamilton et al., 2000; White and
454 Claasen, 1980; Luo and Ebert, 1998). This diffusion process can lead to kinetic isotopic
455 fractionation as the diffusivity of an isotope is a function of its mass (Eq. (5)): light isotopes
456 diffuse more rapidly than heavy ones. It has been shown that Li isotope fractionation can
457 occur during diffusion through silicate melts (Richter et al., 2003; Lundstrom et al., 2005),
458 and in water (Richter et al., 2006). The ratio of ^6Li and ^7Li diffusion coefficients (a) is
459 expressed as:

460

$$461 \quad a = \frac{D_{^7\text{Li}}}{D_{^6\text{Li}}} = \left(\frac{m_{^6\text{Li}}}{m_{^7\text{Li}}} \right)^\beta \quad (6)$$

462

463 The value of the exponent ' β ' is not equal to 0.5, as it would be for a theoretical ideal gas.

464 The value of a (or in other words the β value) must be determined experimentally.

465 The model for determining the a coefficients must take into account not only diffusion
 466 but also dissolution of the hydrated layer. Dissolution occurs either by hydrolysis of ionic-
 467 covalent bonds (Si-O-Si, Si-O-Al) (Bunker, 1994) and/or by metal (Al, Si)-proton exchange
 468 reactions (Oelkers, 2001; Oelkers and Gislason, 2001; Gislason and Oelkers, 2003). The
 469 dissolution process itself does not lead to isotope fractionation, because all of the network
 470 bonds are broken (as supported by the congruent behaviour of elements such as Si, Al, Ca and
 471 Mg (section 3.2)). Consequently, all the Li present in the leached layer is assumed to be
 472 released into solution. Thus, while diffusion results in low $\delta^7\text{Li}$ in solution (relative to the
 473 basaltic glass value), dissolution of the hydrated layer - which is enriched in ^7Li due to
 474 diffusion - tends to increase the $\delta^7\text{Li}$ value of the solution. Since all of our experiments are
 475 performed in closed systems, the maximum $\delta^7\text{Li}$ value for the solution is the fresh basaltic
 476 glass $\delta^7\text{Li}$ value ($+10.3 \pm 0.4\%$) (unless secondary phases are formed).

477 The diffusion coefficient deduced from Eq. (4) is only apparent because Li is also
 478 released by dissolution of the hydrated glass. Dissolution of the glass surface displaces the
 479 surface towards the interior of the glass at a rate r (Boksay et al., 1968). The coordinate x
 480 becomes $x = y - rt$ with $C = 0$ at $x = 0$, x moving at a rate r , and y corresponding to E_{HG} , the
 481 equivalent hydrated glass thickness over which diffusion occurs (Eq. (5)). By differentiation,
 482 $x = y - rt$ becomes:

483

$$484 \left(\frac{\partial x}{\partial t} \right) = \left(\frac{\partial y}{\partial t} \right) - r \quad (7)$$

485

486 Eq. (4) can be expressed as:

487

$$488 \quad \left(\frac{\partial C}{\partial t}\right) = \left(\frac{\partial C}{\partial x}\right)\left(\frac{\partial x}{\partial t}\right) = D\left(\frac{\partial^2 C}{\partial x^2}\right) \quad (8)$$

489

490 It is considered that:

491

$$492 \quad \left(\frac{\partial C}{\partial x}\right) = \left(\frac{\partial C}{\partial y}\right) \quad (9)$$

493

494 By combining Eq. (7), (8) and (9), Eq. (4) becomes:

495

$$496 \quad \left(\frac{\partial C}{\partial y}\right)\left(\frac{\partial y}{\partial t} - r\right) = D\left(\frac{\partial^2 C}{\partial y^2}\right) \quad (10)$$

497

498 and:

499

$$500 \quad \left(\frac{\partial C}{\partial t}\right) = D\left(\frac{\partial^2 C}{\partial y^2}\right) + r\left(\frac{\partial C}{\partial y}\right) \quad (11)$$

501

502 Following the resolution of this equation by Boksay et al. (1968), the solution of Eq. (11) for

503 lithium is:

504

$$505 \quad \frac{dQ_{Li}}{dt} = c \cdot r \cdot (1 - 0.5 \cdot \operatorname{erf}(s)) + c \cdot \sqrt{\frac{D_{Li}}{\pi \cdot t}} \cdot \exp(-s^2) \quad (12)$$

506

507 where dQ_{Li}/dt is the release rate of Li into solution (in $\text{g m}^{-2} \text{d}^{-1}$), r the glass dissolution rate
 508 (in m d^{-1}), c the Li concentration in the bulk glass (in g m^{-3}), D_{Li} the Li diffusion coefficient
 509 (in $\text{m}^2 \text{d}^{-1}$). s is dimensionless and is expressed as:

510

$$511 \quad s = \frac{y - r \cdot t}{\sqrt{4 \cdot D \cdot t}} \quad (13)$$

512

513 Eq. (12) can be numerically integrated in order to determine Q_{Li} . All the parameters
 514 are known except D_{Li} which can be adjusted in order to best fit the data set (by the least
 515 squares method). The total altered glass thickness (y or E_{HG}) is deduced from Eq. (5). The
 516 dissolution rate (r) is determined for each experiment from $NL(\text{Si})$ (Table 5):

517

$$518 \quad r = \frac{dNL(\text{Si})}{dt} = r_0 \cdot \exp\left(-\frac{t}{\tau}\right) \quad (14)$$

519

520 with τ a characteristic time of decrease.

521

522 Therefore:

523

$$524 \quad NL(\text{Si}) = r_0 \cdot \tau \cdot \left(1 - \exp\left(-\frac{t}{\tau}\right)\right) \quad (15)$$

525

526 Note that only the onset of the experiments is considered here (see Table 6). All the calculated
 527 Li diffusion coefficients are detailed in Table 6.

528 Eq. (12) and its numerical integration can also be used to calculate the Li isotopic
 529 composition of the solution. The second step of the modelling consists therefore of fitting the

530 solution $\delta^7\text{Li}$ values (as a function of time) and determining the best value for a (Eq. (6)). This
531 was performed using a least squares method (Fig. 6). The range of uncertainties obtained for
532 the a coefficients was determined so as to cover the whole range of $\delta^7\text{Li}$ values.

533 The best fit for the experiment at 50°C corresponds to a a value of 0.991 ± 0.003 (Fig.
534 6a). At 90°C and pH 3, a is 0.994 ± 0.004 (Fig. 6b). For the experiments at various S/V, the a
535 values are 1.000 ± 0.002 and 0.997 ± 0.002 (Fig. 6c) for S/V = 0.7 and 7 cm⁻¹, respectively.
536 The best fit for the experiment at 90°C is $a = 0.990$ considering all the data, and $a = 0.997 \pm$
537 0.003 without considering the first point (Fig. 6a), which has a much lower pH (as shown in
538 Table 4).

539

540 4.2. Influence of temperature

541

542 It is difficult to assess the role of temperature based on this study alone, since only two
543 temperatures were tested, and since the value obtained for a at 90°C in pure water is
544 associated with a large uncertainty (0.9935 ± 0.005). The $\delta^7\text{Li}$ values of the leachates in the
545 experiment performed at 50°C are lower than in the experiment at 90°C (Fig. 4a). This could
546 be explained by a greater relative contribution of Li from diffusion at 50°C, as highlighted by
547 the particularly low Si/Li in solution (see section 3.4.). In fact, the solution $\delta^7\text{Li}$ depends on
548 the a coefficient (responsible for Li isotope fractionation during diffusion), but also on the
549 relative rate of diffusion and dissolution (see section 4.4). As shown in Fig. 7a, for a given a
550 value of a , various glass dissolution rates can lead to a wide range of $\delta^7\text{Li}$ values.

551 In order to better determine the role of temperature on the a coefficients, we have
552 compiled data available from the literature (Fig. 8). The published data mainly correspond to
553 high-temperature fractionation among silicate minerals, determined experimentally or by field
554 studies. Richter et al. (2003) performed experiments of Li diffusion between rhyolite and

555 basalt at 1350-1450°C and determined a value for the a coefficient of 0.9674. Teng et al.
556 (2006) studied amphibolites and schists of the Tin Mountain pegmatite and determined $a =$
557 0.982 and 0.977 for temperatures ranging between 340 and 600°C. Parkinson et al. (2007)
558 modelled profiles of Li concentrations and isotope compositions measured *in situ* in zoned
559 clinopyroxene and olivine phenocrysts from primitive arc lavas of the New Georgia Group
560 (Solomon Islands) and estimated a values between 0.971 and 0.959 (1050-1100°C).

561 Combining our data with the published values for a as a function of temperature, a
562 relatively good correlation is obtained for diffusion in molten solids ($R^2=0.95$) (Fig. 8) over a
563 large range of temperatures (50-1450°C). A single law can be determined from these data:

564

$$565 \ln(a) = 0.092 \cdot \frac{1000}{RT} - 0.041 \quad (16)$$

566

567 T is the temperature in K and R the ideal gas constant (in $\text{J mol}^{-1} \text{K}^{-1}$).

568 Experiments carried out by Richter et al. (2006) at 75°C ($a = 0.9977$) and Kunze and
569 Fuoss (1962) at 25°C ($a = 0.9965$) also plot on the same trend, although diffusion of lithium
570 occurs in water in both studies (Fig. 8, in grey). The results of Fritz (1992) (reported in
571 Richter et al., 2006) were not used in our compilation as Richter et al. (2006) mentioned that
572 the experimental design uses a dialysis membrane which might induce isotopic fractionation.

573 We suggest that the correlation between temperature and a coefficients is due to a
574 difference in the activation energies (Ea) for ${}^6\text{Li}^+$ and ${}^7\text{Li}^+$ diffusivity (corresponding to an
575 exchange between Li^+ and H^+ for example). The dependency of the diffusion coefficient on
576 temperature would therefore follow an Arrhenius law (McGrail et al., 1984, Chave et al.,
577 2007; Verney-Carron et al., 2010), such that:

578

$$579 \quad a = \frac{D_7}{D_6} = \frac{D_{07} \cdot \exp(-E_{a7} / RT)}{D_{06} \cdot \exp(-E_{a6} / RT)} = a_0 \cdot \exp((E_{a6} - E_{a7}) / RT) \quad (17)$$

580

581 The linear regression of the data (Eq. (16)) shows that the difference between
582 activation energies for ^6Li and ^7Li diffusivity ($E_{a6} - E_{a7}$) is 0.10 ± 0.02 kJ/mol. Although this
583 difference is small, it leads to significant isotope fractionation during diffusion.

584 Overall, the positive correlation highlighted between temperature and a shows that
585 isotopic fractionation caused by diffusion will increase with temperature.

586

587 4.3. Influence of other parameters

588

589 The a values are relatively similar at pH 3-4 (0.994 ± 0.004 , experiment PH3-90) and
590 at pH 8-9 (0.997 ± 0.002 , experiment PH10-90) (Table 6). Therefore, based on our data, pH
591 has no obvious effect on diffusion induced Li isotope fractionation. In contrast, the rate of Li
592 diffusion and the rate of glass dissolution are expected to vary with pH. Basaltic glass
593 dissolution rates increase as pH decreases, but are also elevated toward alkaline pH. The
594 evolution of the dissolution rate as a function of pH displays a U-shape with a minimum at
595 around pH 4-6 (Guy and Schott, 1989; Gislason and Oelkers, 2003). Guy and Schott (1989)
596 have shown that in the acidic pH region, dissolution is promoted by adsorption of H^+ on Al
597 and Fe surface sites, whereas in the alkaline pH region, dissolution is promoted by the
598 adsorption of OH^- on Si sites. According to Guy and Schott, (1989), the dissolution rate at
599 100°C is 1.6×10^{-7} molSi/m²/s at pH 3, and 9.8×10^{-7} molSi/m²/s at pH 8.6 whereas Gislason
600 and Oelkers (2003) measured different values at 100°C : 2.5×10^{-8} molSi/m²/s at pH 3, and 5.2
601 $\times 10^{-8}$ molSi/m²/s at pH 8.6. However, both studies show that the dissolution rate is lower at
602 pH 3 than at pH 8.6, in agreement with our data (see r_0 in Table 6).

603 In contrast to silicate dissolution rates, the Li diffusion coefficient is expected to
604 increase as pH decreases (White and Claasen, 1980; Bunker, 1994; Chave et al., 2007;
605 Verney-Carron et al., 2010), because ion exchange (assumed to be responsible for the
606 diffusion of alkalis during alteration) depends on the H^+ concentration in solution. However,
607 in the experiments performed at pH 3, the estimated Li diffusion is surprisingly low.

608 The S/V ratio appears to have an effect on the a ratio (Fig. 6c), since SV1 and SV2
609 experiments lead to contrasting a values (1 and 0.997, respectively). However, these
610 experiments were longer than the low S/V experiments and may be affected by secondary
611 phase formation. For both SV1 and SV2 experiments, saturation (Si \sim 15 mg/L) was reached
612 quickly, after 20 days. Nevertheless, in order to obtain the same Si concentration in solution,
613 10 times more glass had to be altered in the experiment with $S/V = 0.7 \text{ cm}^{-1}$ (SV1) compared
614 with SV2 which contained 10 times less glass in the beaker. This suggests that more
615 secondary minerals, potentially incorporating Li, could have precipitated during experiment
616 SV1. Since at 90°C the isotope fractionation using Li incorporation into clays can be
617 significant (e.g. -10‰ for smectites, Vigier et al., 2008), this effect could also explain the
618 higher $\delta^7\text{Li}$ in the leachates of experiment SV1.

619 In summary, we show that the a parameter for Li isotope fractionation during diffusion
620 seems to be primarily influenced by temperature. Also, we show that, at a given temperature,
621 the relative diffusion and dissolution contributions can significantly affect the Li isotope
622 composition of the solution.

623

624 **4.4. Implications for natural systems**

625

626 The results of this study have shown that weathering of basaltic glass cannot lead to an
627 enrichment in ^7Li of the solution, which suggests that high $\delta^7\text{Li}$ values in river waters draining
628 basalts must be due to the preferential uptake of ^6Li by secondary phases.

629 The data also reveal the importance of diffusion-driven Li isotope fractionation under
630 conditions that inhibit secondary phase precipitation. The temperature dependency of this
631 isotope fractionation (α ratio) (Fig. 8) indicates a greater potential effect at high temperatures,
632 such as those that have been measured in hydrothermal fluids (α ranges between 0.985 and
633 0.979 for 150-350°C). However, this effect is not directly demonstrated by $\delta^7\text{Li}$ measured in
634 hydrothermal fluids, which are systematically higher than $\delta^7\text{Li}$ determined for fresh MORB
635 (the average $\delta^7\text{Li}$ for hydrothermal fluids is $\sim +8.1 \pm 1.8$ ‰, Chan and Edmond, 1988; Chan
636 et al., 1993, 1994; Foustoukos et al., 2004; Millot et al., 2010).

637 In fact, the Li isotope compositions of solutions also depend on the relative
638 contribution of diffusion and dissolution. At high temperatures, the release rate of Li from
639 solid phases is high, resulting in the high Li contents of hydrothermal fluids (Seyfried et al.,
640 1984; Berger et al., 1988). The initial dissolution rate (r_0) and Li diffusion coefficients (D)
641 calculated from the experiments performed at 50 and 90°C (PW-50 and PW-90) can be
642 extrapolated to lower and higher temperatures by using an Arrhenius law. Thus, the activation
643 energies of diffusion and dissolution are found to be 102 and 110 kJ mol $^{-1}$, respectively.
644 These values are slightly higher than published data for basaltic glass (e.g. Techer et al.,
645 2000) and show that the relative contribution of diffusion compared to dissolution decreases
646 as temperature increases. In other words, r_0/D increases as a function of temperature. Fig. 7b
647 displays the initial stages of the $\delta^7\text{Li}$ temporal evolution in solution at various temperatures
648 (from 50 to 120°C) (following the model developed in section 4.1) At temperatures higher
649 than 120°C, the contribution of dissolution is high and masks the effect of isotope
650 fractionation occurring during diffusion of Li through the leached layer. The model also

651 predicts that at temperatures between 50 and 90°C, the role of diffusion dominates over
652 dissolution, resulting in solution $\delta^7\text{Li}$ which are lower than the fresh glass value. At lower
653 temperatures (< 50°C), the solution $\delta^7\text{Li}$ goes back towards the fresh basaltic glass value,
654 since the isotope fractionation occurring during diffusion becomes negligible (α close to 1).
655 Overall, these simulations highlight that the solution $\delta^7\text{Li}$, in absence of secondary mineral
656 formation, strongly depends on temperature since this parameter influences the dissolution
657 rate, the diffusion coefficients, and the Li isotope fractionation factor. Also, the S/V ratio
658 which can be related to parameters such as water/rock ratio, porosity and specific surface area
659 plays a key role, as it can drastically change the relative contribution of diffusion and
660 dissolution. In the field, these parameters should therefore influence the Li isotope
661 composition of the fluids before formation of any secondary minerals starts. In models, the
662 initial composition of the fluid may therefore not be strictly equal to the isotope composition
663 of the fresh rock or minerals that it drains.

664 In summary, diffusion should not play a significant role in low-temperature natural
665 systems as the isotope fractionation factor is close to 1. In high temperature hydrothermal
666 systems, the dissolution rates are significant and may entirely mask the effect of diffusion.
667 However, the role of diffusion should be taken into account for modelling alteration processes
668 occurring at moderate temperatures.

669

670

5. SUMMARY AND CONCLUSIONS

671

672 The results of basaltic glass alteration experiments performed at various temperatures
673 (50 and 90°C), various pH (3 and around 9) and various S/V ratio (0.7 and 7 cm⁻¹) have
674 shown that the alteration of basaltic glass at far from equilibrium conditions produces a
675 solution with a lighter Li isotopic composition than the starting material. This challenges the

676 idea that the weathering of silicate glasses could preferentially release ^7Li into rivers. The Li
677 isotopic composition of the solution can be modeled in terms of mass-dependent isotope
678 fractionation of Li, as Li diffuses through the hydrated glass into solution. This fractionation
679 can be explained by a difference in the diffusion coefficients of ^6Li and ^7Li . The ratio a ,
680 defined as the ratio of these diffusion coefficients ($a = D_7/D_6$), decreases as a function of
681 temperature. The relationship between a and temperature appears to follow an Arrhenius' law,
682 and may be related to a difference in the activation energies of the $^6\text{Li}^+$ and $^7\text{Li}^+$ diffusivity.
683 These results can help to interpret the Li isotope signatures of natural systems. Without
684 considering the role of secondary mineral formation it seems that the effect of diffusion on the
685 Li isotopic composition is not negligible for systems where water rock interactions occur at
686 moderate temperatures (50-100°C).

687

688

ACKNOWLEDGEMENTS

689

690 We would like to thank S. Gin and P. Jollivet (CEA, LCLT) for supplying the synthetic
691 basaltic glass. We also thank D. Yechigeyan, J. and L. Marin (SARM) for chemical
692 analyses. We are grateful to M. Champenois, D. Mangin and C. Rollion-Bard (CRPG) for
693 their technical help with the SIMS. We also would like to acknowledge S. Alfaro (LISA)
694 for his help with the model and P. Burnard (CRPG) for English corrections. J.C. Alt, R.H.
695 James and an anonymous reviewer are sincerely thanked for their comments that help to
696 improve this manuscript. This is CRPG contribution # 2113.

ACCEPTED MANUSCRIPT

REFERENCES

- 697
698
- 699 Aagard P. and Helgeson H.C. (1982) Thermodynamic and kinetic constraints on reaction rates
700 among minerals and aqueous solutions. I. Theoretical considerations. *Am. J. Sci.* **282**, 237-
701 285.
- 702 Berger G., Schott J. and Guy C. (1988). Behavior of Li, Rb and Cs during basalt glass and
703 olivine dissolution and chlorite, smectite and zeolite precipitation from seawater:
704 Experimental investigations and modelization between 50° and 300°C. *Chem. Geol.* **71**,
705 297-312.
- 706 Berger G., Claparols C., Guy C. and Daux V. (1994) Dissolution rate of a basalt glass in silica-
707 rich solutions: Implications for long-term alteration. *Geochim. Cosmochim. Acta* **58**, 4875-
708 4886.
- 709 Boksay Z., Bouquet G. and Dobos S. (1968) The kinetics of leached layers on glass surfaces.
710 *Phys. Chem. Glasses* **9**, 69-71.
- 711 Bunker B.C. (1994) Molecular mechanisms for corrosion of silica and silicate glasses. *J. Non-
712 Cryst. Solids* **179**, 300-308.
- 713 Carignan J., Vigier N. and Millot R. (2007) Three secondary reference materials for Li
714 isotope measurements: Li7-N, Li6-N and LiCl-N solutions. *Geostand. Geoanal. Res.* **31**,
715 7-12.
- 716 Chan L.H. and Edmond J.M. (1988) Variation of lithium isotope composition in the marine
717 environment: a preliminary report. *Geochim. Cosmochim. Acta* **52**, 1711-1717.
- 718 Chan L.H., Edmond J.M., Thompson G. and Gillis K. (1992) Lithium isotopic composition of
719 submarine basalts: implications for the lithium cycle to the ocean. *Earth Planet. Sci. Lett.*,
720 **108**, 151-160.

- 721 Chan L.H., Edmond J.M. and Thompson G. (1993) A lithium isotope study of hot springs and
722 metabasalts from mid ocean ridge hydrothermal systems. *J. Geophys. Res.* **98**, 9653-9659.
- 723 Chan L.H., Gieskes J.M., You C.F. and Edmond J.M. (1994) Lithium isotope geochemistry of
724 sediments and hydrothermal fluids of the Gaymas Basin, Gulf of California. *Geochim.*
725 *Cosmochim. Acta* **58**, 4443-4454.
- 726 Chan L.H., Alt J.C. and Teagle D.A.H. (2002) Lithium and lithium isotope profiles through
727 the upper oceanic crust: a study of seawater-basalt exchange at ODP Sites 504B and
728 896A. *Earth Planet. Sci. Lett.* **201**, 187-201.
- 729 Chaussidon M. and Robert F. (1998) $^7\text{Li}/^6\text{Li}$ and $^{11}\text{B}/^{10}\text{B}$ variations in chondrules from the
730 Semarkona unequilibrated chondrite. *Earth Planet. Sci. Lett.* **164**, 577-589.
- 731 Chave T., Frugier P., Ayrat A. and Gin S. (2007) Solid state diffusion during nuclear glass
732 residual alteration in solution. *J. Nucl. Mater.* **362**, 466-473.
- 733 Crovisier J.L., Advocat T. and Dussossoy J.L. (2003) Nature and role of natural alteration gels
734 formed on the surface of ancient volcanic glasses (Natural analogs of waste containment
735 glasses). *J. Nucl. Mater.* **321**, 91-109.
- 736 Daux V., Guy C., Advocat T., Crovisier J.L. and Stille P. (1997) Kinetic aspects of basaltic
737 glass dissolution at 90°C: role of aqueous silicon and aluminium. *Chem. Geol.* **142**,
738 109-126.
- 739 Dessert C., Dupré B., Gaillardet J., François L. and Allègre C.J. (2003) Basalt weathering
740 laws and the impact of basalt weathering on the global carbon cycle. *Chem. Geol.* **202**,
741 257-273.
- 742 Dupré B., Dessert C., Oliva P., Goddérès Y., Viers J., François L., Millot R. and Gaillardet J.
743 (2003) Rivers, chemical weathering and Earth's climate. *C.R. Geoscience* **335**, 1141-1160.
- 744 Flesch G.D., Anderson A.R. and Svec H.J. (1973) A secondary isotopic standard for $^6\text{Li}/^7\text{Li}$
745 determinations. *Int. J. Mass Spectrom. Ion Phys.* **12**, 265-272.

- 746 Franck S., Bounama C. and von Bloh W. (2008) Weathering. In *Encyclopedia of Ecology*,
747 3770-3776.
- 748 Frugier P., Gin S., Minet Y., Chave T., Bonin B., Godon N., Lartigue J.E., Jollivet P., Ayrat A.,
749 De Windt L. and Santarini G. (2008) SON68 nuclear glass dissolution kinetics: Current
750 state of knowledge and basis of the new GRAAL model. *J. Nucl. Mater.* **380**, 8-21.
- 751 Frugier P., Chave T., Lartigue J.E. and Gin S. (2009) Application of the GRAAL model to
752 leaching experiments with SON68 nuclear glass in initially pure water. *J. Nucl. Mater.* **392**,
753 552-567.
- 754 Gaillardet J., Dupré B., Louvat P. and Allègre C.J. (1999) Global silicate weathering and CO₂
755 consumption rates deduced from the chemistry of large rivers. *Chem. Geol.* **159**, 3-30.
- 756 Gislason S.R. and Oelkers E.H. (2003) Mechanism, rates, and consequences of basaltic glass
757 dissolution: II. An experimental study of the dissolution rates of basaltic glass as a
758 function of pH and temperature. *Geochim. Cosmochim. Acta* **67**, 3817-3832.
- 759 Grambow B. (1985) A general rate equation for nuclear waste glass corrosion. *Mat. Res. Soc.*
760 *Symp. Proc.* **44**, 15-27.
- 761 Guy C. and Schott J. (1989) Multisite surface reaction versus transport control during the
762 hydrolysis of a complex oxide. *Chem. Geol.* **78**, 181-204.
- 763 Hamilton J.P., Pantano C.G. and Brantley S.L. (2000) Dissolution of albite glass and crystal.
764 *Geochim. Cosmochim. Acta* **64**, 2603-2615.
- 765 Hartmann J., Jansen N., Dürr H.H., Kempe S. and Köhler P. (2009) Global CO₂-consumption
766 by chemical weathering: What is the contribution of highly active weathering regions?
767 *Global Planet. Change* **69**, 185-194.
- 768 Hoefs J. and Sywall M. (1997) Lithium isotopic composition of Quaternary and Tertiary
769 biogene carbonates and a global lithium isotope balance. *Geochim. Cosmochim. Acta* **61**,
770 2679-2690.

- 771 Huh Y., Chan L.C., Zhang L. and Edmond J.M. (1998) Lithium and its isotopes in major
772 world rivers: implications for weathering and the oceanic budget. *Geochim. Cosmochim.*
773 *Acta* **62**, 2039-2051.
- 774 Huh Y., Chan L.C. and Edmond J.M. (2001) Lithium isotopes as a probe of weathering
775 processes: Orinoco River. *Earth Planet. Sci. Lett.* **194**, 189-199.
- 776 Huh Y., Chan L.C. and Chadwick O.A. (2004) Behavior of lithium and its isotopes during
777 weathering of Hawaiian basalt. *Geochem. Geophys. Geosyst.* **5**, 1-22.
- 778 James R.H., Allen D.E. and Seyfried, W.E. Jr. (2003) An experimental study of alteration of
779 oceanic crust and terrigenous sediments at moderate temperatures (51 to 350°C): Insights
780 as to chemical processes in ear-shore ridge-flank hydrothermal systems. *Geochim.*
781 *Cosmochim. Acta* **67**, 681-691.
- 782 Kiskürek B., Widdowson M. and James R.H. (2004) Behaviour of Li isotopes during
783 continental weathering: the Bidar laterite profile, India. *Chem. Geol.* **212**, 27-44.
- 784 Kiskürek B., James R.H. and Harris N.B.W. (2005) Li and $\delta^7\text{Li}$ in Himalayan rivers: Proxies
785 for silicate weathering? *Earth Planet. Sci. Lett.* **237**, 387-401.
- 786 Kunze R.W. and Fuoss R.M. (1962) Conductance of the alkali halides. III. The isotopic
787 lithium chlorides. *J. Phys. Chem.* **66**, 930-931.
- 788 Lemarchand E., Chabaud F., Vigier N., Millot R. and Pierret M.C. (2010) Lithium isotope
789 systematics in a forested granitic catchment (Strengbach, Vosges Mountains, France).
790 *Geochim. Cosmochim. Acta*, in press.
- 791 Lerman A., Wu L. and Mackenzie F.T. (2007) CO_2 and H_2SO_4 consumption in weathering
792 and material transport to the ocean, and their role in the global carbon balance. *Marine*
793 *Chem.* **106**, 326-350.

- 794 Louvat P. and Allègre C.J. (1997) Present denudation rates on the island of Réunion
795 determined by river geochemistry: Basalt weathering and mass budget between chemical
796 and mechanical erosions. *Geochim. Cosmochim. Acta* **61**, 3645-3669.
- 797 Louvat P. and Allègre C.J. (1998) Riverine erosion rates on Sao Miguel volcanic island,
798 Azores archipelago. *Chem. Geol.* **148**, 177-200.
- 799 Ludwig W., Amiotte-Suchet P. and Probst J.L. (1999) Enhanced chemical weathering of
800 rocks during the last glacial maximum: a sink for atmospheric CO₂? *Chem. Geol.* **159**,
801 147-161.
- 802 Lundstrom C.C., Chaussidon M., Hsui A.T., Kelemen P. and Zimmerman M. (2005)
803 Observations of Li isotopic variations in the Trinity Ophiolite: Evidence for isotopic
804 fractionation by diffusion during mantle melting. *Geochim. Cosmochim. Acta* **69**, 735-
805 751.
- 806 Luo J.S. and Ebert W.L. (1998) Examination of subaerially altered basaltic glass with TEM
807 and EELS. *Am. Ceramic Soc. Proc.*, 8 pp.
- 808 McGrail B.P., Kumar A. and Day D.E. (1984) Sodium Diffusion and Leaching of Simulated
809 Nuclear Waste Glass. *J. Am. Ceram. Soc.* **67**, 463-467.
- 810 Millot R., Guerrot C. and Vigier N. (2004) Accurate and high-precision measurement of
811 lithium isotopes in two reference materials by MC-ICP-MS. *Geostand. Geoanal. Res.* **28**,
812 153-159.
- 813 Millot R., Scaillet B. and Sanjuan B. (2010a) Lithium isotopes in island arc geothermal
814 systems: Guadeloupe, Martinique (French West Indies) and experimental approach.
815 *Geochim. Cosmochim. Acta* **74**, 1852-1871.
- 816 Millot R., Vigier N. and Gaillardet, J. (2010b) Behaviour of lithium and its isotopes during
817 weathering in the Mackenzie Basin, Canada. *Geochim. Cosmochim. Acta*, **74**, 3897-3912.

- 818 Millot R., Petelet-Giraud E., Guerrot C. and Négrel P. (2010c) Multi-isotopic composition
819 ($\delta^7\text{Li}$ - $\delta^{11}\text{B}$ - δD - $\delta^{18}\text{O}$) of rainwaters in France: Origin and spatio-temporal characterization.
820 *Applied Geochem.* **25**, 1510-1524.
- 821 Oelkers E.H. (2001) General kinetic description of multioxide silicate mineral and glass
822 dissolution. *Geochim. Cosmochim. Acta* **65**, 3703-3719.
- 823 Oelkers E.H. and Gislason S.R. (2001) The mechanism, rates, and consequences of basaltic
824 glass dissolution: I. An experimental study of the dissolution rates of basaltic glass as a
825 function of aqueous Al, Si and oxalic acid concentration at 25°C and pH = 3 and 11.
826 *Geochim. Cosmochim. Acta* **65**, 3671-3681.
- 827 Parkinson I.J., Hammond S.J., James R.H. and Rogers N.W. (2007) High-temperature lithium
828 isotope fractionation: Insights from lithium isotope diffusion in magmatic systems. *Earth*
829 *Planet. Sci. Lett.* **257**, 609-621.
- 830 Pistiner J.S. and Henderson G.M. (2003) Lithium isotope fractionation during continental
831 weathering processes. *Earth Planet. Sci. Lett.* **214**, 327-339.
- 832 Pogge von Strandmann P.A.E., James R.H., van Calsteren P., Gislason S.R. and Burton K.W.
833 (2008) Lithium, magnesium and uranium isotope behaviour in the estuarine environment
834 of basaltic islands. *Earth Planet. Sci. Lett.* **274**, 462-471.
- 835 Pogge von Strandmann P.A.E., Burton K.W., James R.H., van Calsteren P. and Gislason S.R.
836 (2010) Assessing the role of climate on uranium and lithium isotope behaviour in rivers
837 draining a basaltic terrain. *Chem. Geol.* **270**, 227-239.
- 838 Rana M.A. and Douglas R.W. (1961a) The Reaction Between Glass and Water. Part 1.
839 Experimental Methods and Observations. *Phys. Chem. Glasses* **2**, 179-195.
- 840 Rana M.A. and Douglas R.W. (1961b) The Reaction Between Glass and Water. Part 2.
841 Discussion of the Results. *Phys. Chem. Glasses* **2**, 196-204.

- 842 Richter F.M., Davis A.M., DePaolo D.J. and Watson E.B. (2003) Isotope fractionation by
843 chemical diffusion between molten basalt and rhyolite. *Geochim. Cosmochim. Acta* **67**,
844 3905-3923.
- 845 Richter F.M., Mendybaev R.A., Christensen J.N., Hutcheon I.D., Williams R.W., Sturchio
846 N.C. and Beloso A.D. Jr. (2006) Kinetic isotopic fractionation during diffusion of ionic
847 species in water. *Geochim. Cosmochim. Acta* **70**, 277-289.
- 848 Rudnick R.L., Tomascak P.B., Njo H.B. and Robert Gardner L. (2004) Extreme lithium
849 isotopic fractionation during continental weathering revealed in saprolites from South
850 Carolina. *Chem. Geol.* **212**, 45-57.
- 851 Schiano P., Birck J.L., Allègre C.J. (1997) Osmium-strontium-neodymium-lead isotopic
852 covariations in mid-ocean ridge basalt glasses and the heterogeneity of the upper mantle.
853 *Earth Planet. Sci. Lett.* **150**, 363-379.
- 854 Seyfried W.E. Jr., Janecky D.R. and Mottl M.J. (1984) Alteration of the oceanic crust:
855 implications for the geochemical cycles of lithium and boron. *Geochim. Cosmochim. Acta*
856 **48**, 557-569.
- 857 Seyfried W.E. Jr., Chen X. and Chan L.H. (1998) Trace element mobility and lithium isotope
858 exchange during hydrothermal alteration of seafloor weathered basalt: An experimental
859 study at 350°C, 500 bars. *Geochim. Cosmochim. Acta* **62**, 949-960.
- 860 Stroncik N.A. and Schmincke H.U. (2001) Evolution of palagonite: Crystallization, chemical
861 changes, and element budget. *Geochem. Geophys. Geosyst.* **2**, 1017.
- 862 Techer I., Advocat T., Lancelot J. and Liotard J.M. (2000) Basaltic glass: alteration
863 mechanisms and analogy with nuclear waste glasses. *J. Nucl. Mater.* **282**, 40-46.
- 864 Techer I., Advocat T., Lancelot J., Liotard J.M. (2001) Dissolution kinetics of basaltic glasses:
865 control by solution chemistry and protective effect of the alteration film. *Chem. Geol.* **176**,
866 235-263.

- 867 Teng F.Z., McDonough W.F., Rudnick R.L., Dalpé C., Tomascak P.B., Chappell B.W. and
868 Gao S. (2004) Lithium isotopic composition and concentration of the upper continental
869 crust. *Geochim. Cosmochim. Acta* **68**, 4167-4178.
- 870 Teng F.Z., McDonough W.F., Rudnick R.L. and Walker R.J. (2006) Diffusion-driven extreme
871 lithium isotopic fractionation in country rocks of the Tin Mountain pegmatite. *Earth
872 Planet. Sci. Lett.* **243**, 701-710.
- 873 Teng F.Z., Rudnick R.L., McDonough W.F., Gao S., Tomascak P.B. and Liu Y. (2008)
874 Lithium isotopic composition and concentration of the deep continental crust. *Chem.
875 Geol.* **255**, 47-59.
- 876 van der Lee J. and De Windt L. (2002) *CHESS Tutorial and Cookbook. Updated for version
877 3.0.* École des Mines de Paris, Centre d'Informatique Géologique, Fontainebleau, France.
- 878 Verney-Carron A., Gin S., Frugier P. and Libourel G. (2010) Long-term modeling of
879 alteration-transport coupling: Application to a fractured Roman glass. *Geochim.
880 Cosmochim. Acta* **74**, 2291-2315.
- 881 Vigier N., Burton K.W., Gislason S.R., Rogers N.W., Duchene S., Thomas L., Hodge E. and
882 Schaefer B. (2006) The relationship between riverine U-series disequilibria and erosion
883 rates in a basaltic terrain. *Earth Planet. Sci. Lett.* **249**, 258-273.
- 884 Vigier N., Decarreau A., Millot R., Carignan J., Petit S. and France-Lanord C. (2008)
885 Quantifying Li isotope fractionation during smectite formation and implications for the Li
886 cycle. *Geochim. Cosmochim. Acta* **72**, 780-792.
- 887 Vigier N., Gislason S.R., Burton K.W., Millot R. and Mokadem F. (2009) The relationship
888 between riverine lithium isotope composition and silicate weathering rates in Iceland.
889 *Earth Planet. Sci. Lett.* **287**, 434-441.
- 890 White A.F., Claasen H.C. (1980) Kinetic model for the short-term dissolution of a rhyolitic
891 glass. *Chem. Geol.* **28**, 91-109.

- 892 Williams L.B. and Hervig R.L. (2005) Lithium and boron isotopes in illite-smectite: the
893 importance of crystal size. *Geochim. Cosmochim. Acta* **69**, 5705-5716.
- 894 Wimpenny J., Gislason S.R., James R.H., Gannoun A., Pogge von Strandmann P.A.E. and
895 Burton K. (2010) The behaviour of Li and Mg isotopes during primary phase dissolution
896 and secondary mineral formation in basalt. *Geochim. Cosmochim. Acta*, in press.
- 897 Wolery T. (1992) *EQ3/6, A Software Package for Geochemical Modeling of Aqueous*
898 *Systems: Package overview and Installation Guide (Version 7.0.)*. Lawrence Livermore
899 National Laboratory Report, UCRL-MA-110662 PT1.
- 900 Wolff-Boenisch D., Gislason S.R., Oelkers E. H. and Putnis C.V. (2004) The dissolution rates
901 of natural glasses as a function of their composition at pH 4 and 10.6, and temperatures
902 from 25 to 74°C. *Geochim. Cosmochim. Acta* **68**, 4843-4858.
- 903 Wolff-Boenisch D., Gislason S.R. and Oelkers E. H. (2006) The effect of cristallinity on
904 dissolution rates and CO₂ consumption capacity of silicates. *Geochim. Cosmochim. Acta*
905 **70**, 858-870.
- 906 Zhang L., Chan L.H. and Gieskes J.M. (1998) Lithium isotope geochemistry of pore waters
907 from Ocean Drilling Program Sites 918 and 919, Irminger Basin. *Geochim. Cosmochim.*
908 *Acta* **62**, 2437-2450.
- 909

Figure captions

Figure 1. Evolution of Si (a) and Li (b) concentrations in solution with time for all the experiments performed at 90°C (see Table 4).

Figure 2. Normalized mass losses (Eq. (2)) of Ca, Al, Si, Mg, Na, and Li during alteration for the experiment in pure water at 90°C (PW-90). The solid line represents a fit of the normalized mass losses for alkalis (see Eq. (5)) using a square root function and the dashed line corresponds to a fit of the normalized mass losses for the other elements using two linear functions.

Figure 3. (a) Determination of the 'initial' dissolution rate (r_0) for the experiments in pure water at 90°C (PW-90) and 50°C (PW-50) using Eq. (3). The initial dissolution rate is deduced from the slope of the linear regression on $dNL(Si)/dt$. (b) Determination of the Li diffusion coefficient (D) for the experiments in pure water at 90°C (PW-90) and 50°C (PW-50) using Fick's second law (Eq. (5)). The slope of the linear regression on $dNL(Li)/dt$ corresponds to $2\rho\sqrt{Dt}$.

Figure 4. Evolution of the Li isotopic composition of the leachate solutions (δ^7Li) with time: (a) for the experiments at 90°C and 50°C (in pure water and $S/V = 0.7 \text{ cm}^{-1}$), (b) at pH 3 and 9 (at 90°C and $S/V = 0.7 \text{ cm}^{-1}$), (c) at S/V of 0.7 and 7 cm^{-1} (in pure water and 90°C). The thick black line corresponds to the fresh synthetic basaltic glass value with its uncertainties in grey.

Figure 5. Schematic view of the diffusion - dissolution model described in the text. The alteration process is considered as two processes: formation of a leached layer by interdiffusion between alkalis and protons and dissolution of the leached layer.

Figure 6. Modeling the experiments: (a) at 90 and 50°C (in pure water and $S/V = 0.7 \text{ cm}^{-1}$), (b) at pH 3 (90°C and $S/V = 0.7 \text{ cm}^{-1}$), (c) at S/V of 0.7 and 7 cm^{-1} (in pure water and 90°C). The thick black horizontal line corresponds to the fresh synthetic basaltic glass value with uncertainties in grey. The curves correspond to the fit of the data with the a value determined from the least square method.

Figure 7. Simulation of δ^7Li values of the leaching solution of the synthetic basaltic glass as a function of time: (a) at 90°C by considering the measured values of D and r_0 , $r_0/10$, $r_0/100$; (b) at various temperatures (between 20 and 120°C). The results are obtained from Eq. (12) and (13) and by considering r_0 and D extrapolated from our measured data to 50 and 90°C. The a ratio is calculated from Eq. (16).

Figure 8. Logarithm of the a ratio as a function of the inverse of the temperature. R is the ideal gas constant. According to Arrhenius' law and Eq. (17), the slope corresponds to the difference of activation energies for diffusion of 6Li and 7Li , respectively.

Figure 1

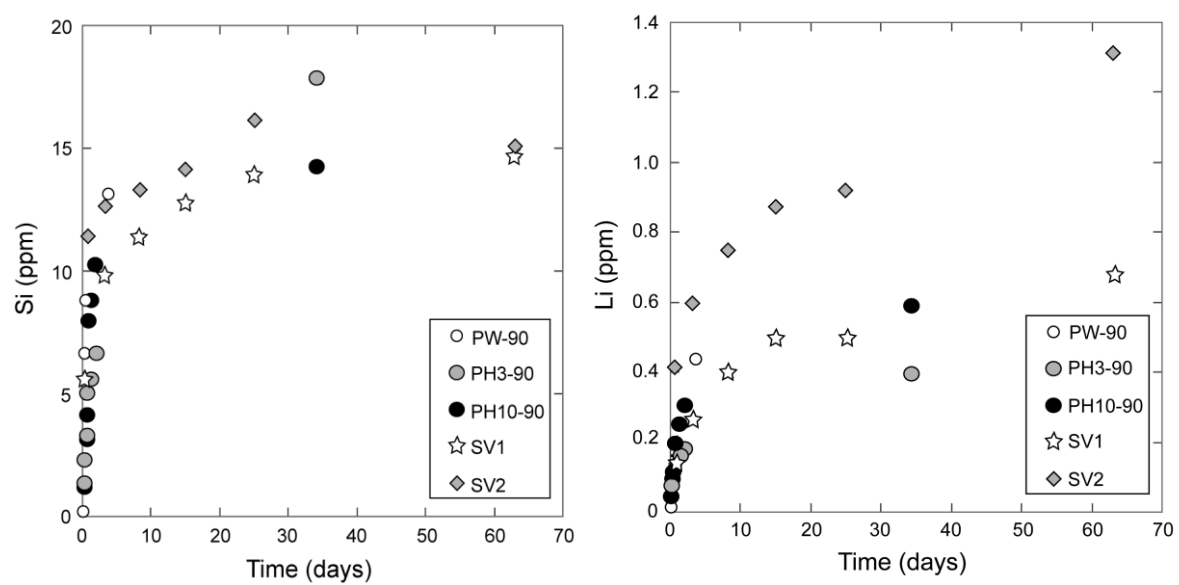


Figure 2

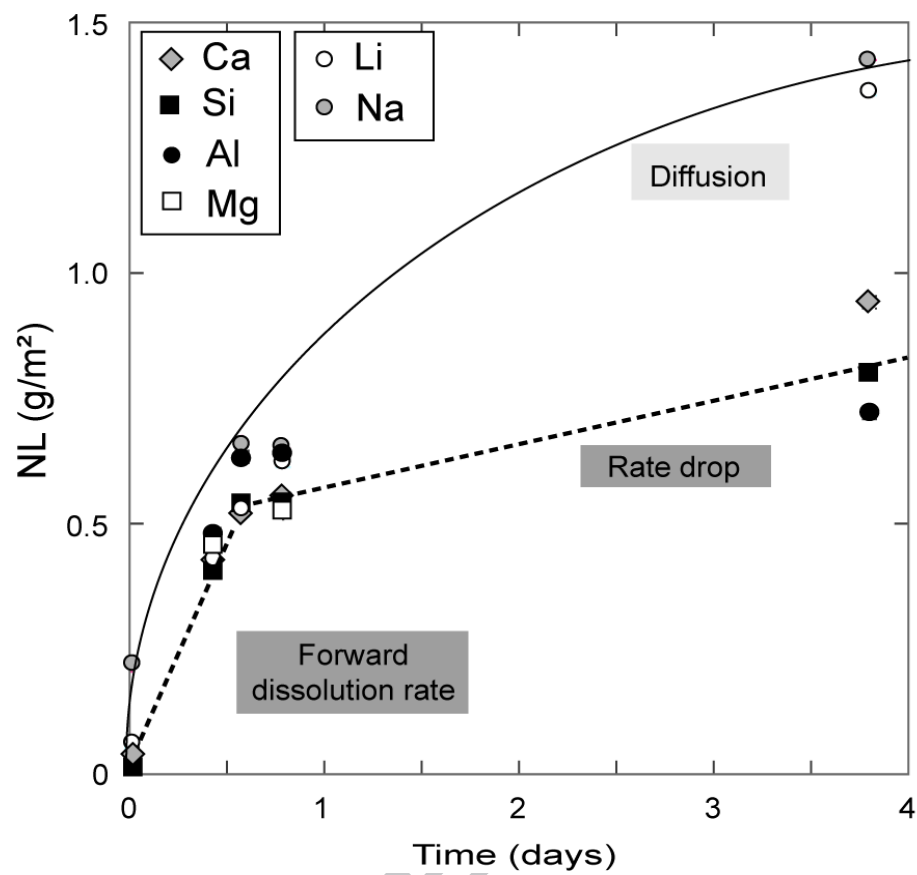


Figure 3

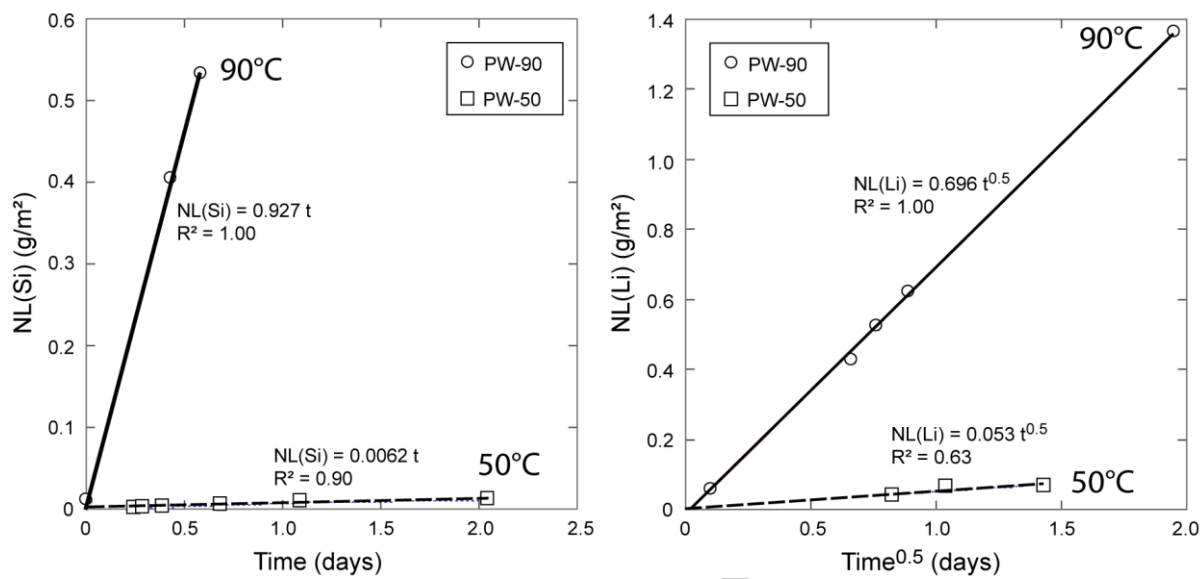


Figure 4

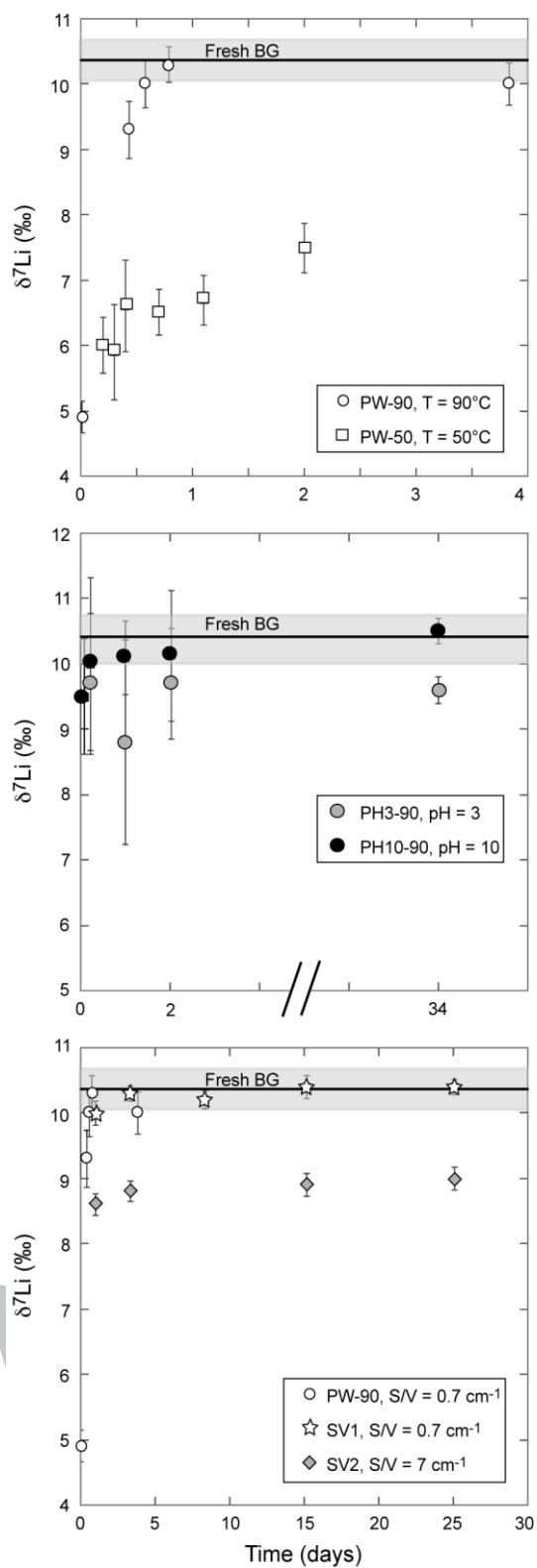


Figure 5

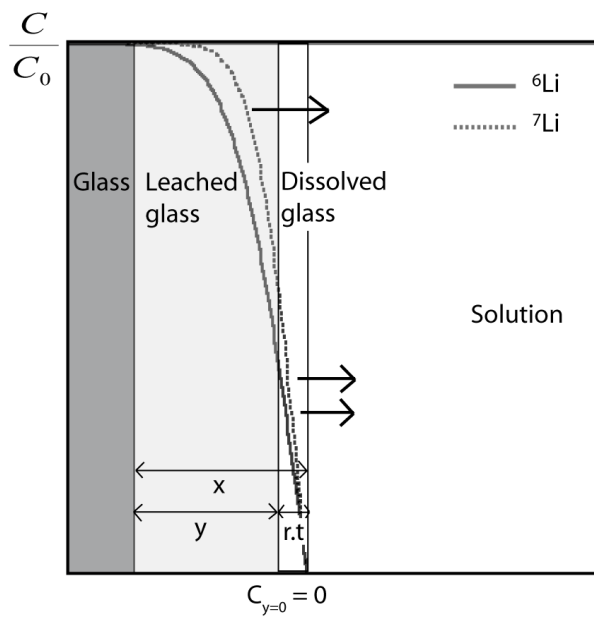


Figure 6

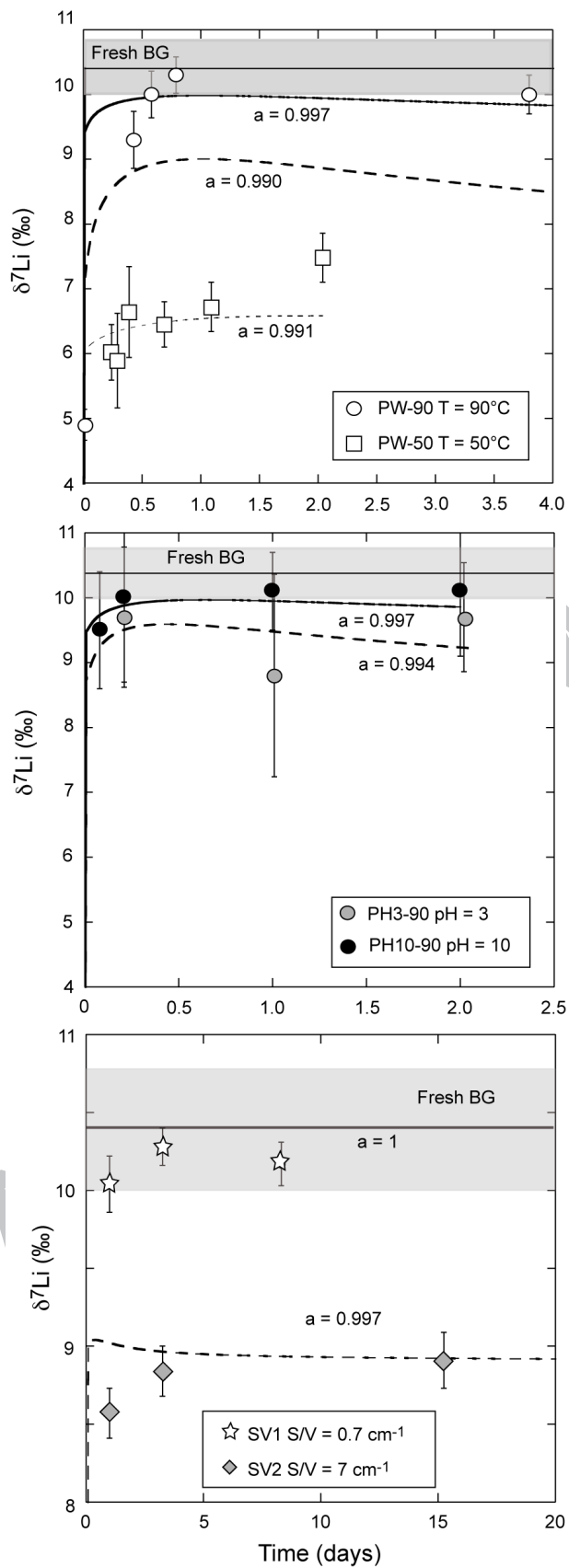


Figure 7.

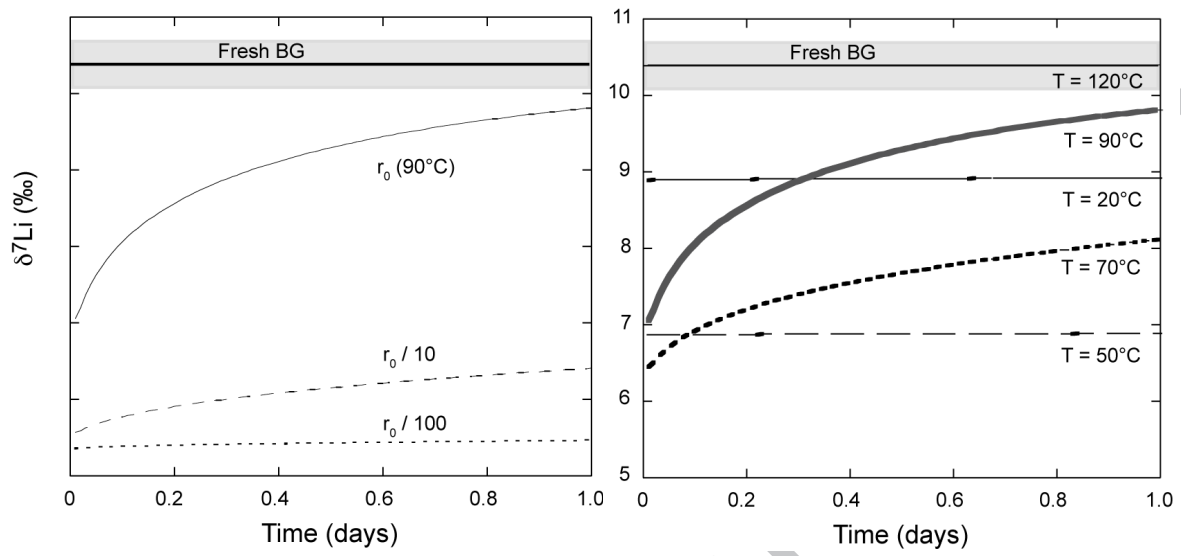


Figure 8.

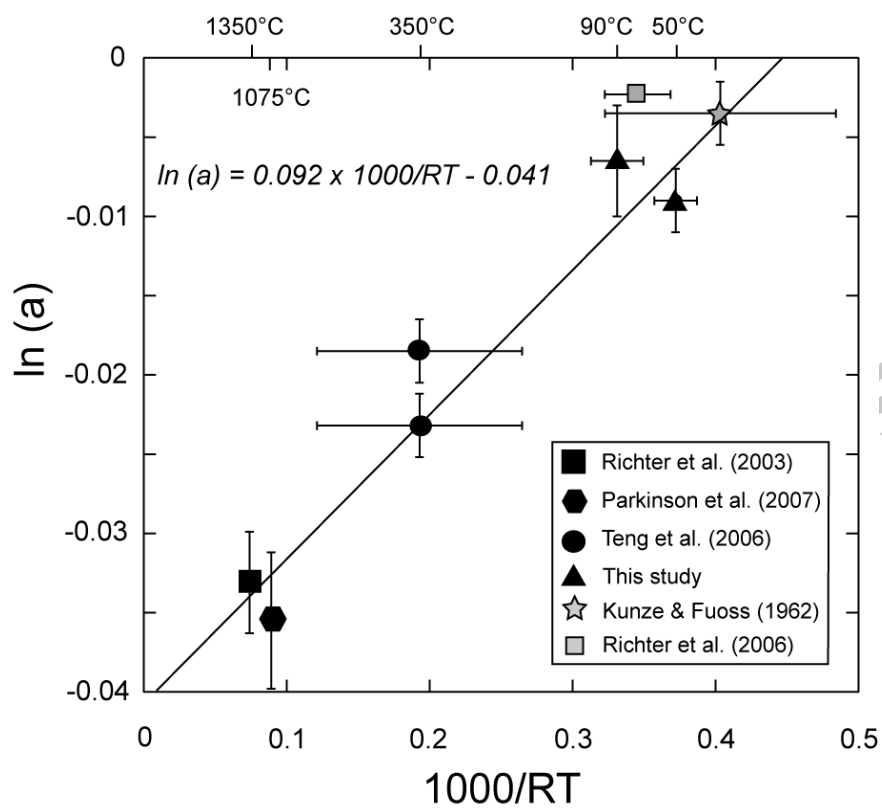


Table 1. Summary of experimental conditions.

Exp. name	Temp. °C	Solution	BG* mass g	Sol. volume mL	S/V** cm ⁻¹	Time days
PW-90-t1	90	Pure water	0.042	50.4	0.70	0.02
PW-90-t2	90	Pure water	0.042	50.1	0.71	0.42
PW-90-t3	90	Pure water	0.043	50.1	0.72	0.58
PW-90-t4	90	Pure water	0.042	50.0	0.71	0.79
PW-90-t5	90	Pure water	0.042	50.0	0.71	4
PH3-90	90	0.001M HCl (pH 3 at 25°C)	0.168	200.2	0.71	0.08, 0.21, 0.33, 1, 1.3, 2, 34
PH10-90	90	0.0001M NaOH (pH 10 at 25°C)	0.168	199.8	0.71	0.08, 0.21, 0.33, 1, 1.3, 2, 34
SV1	90	Pure water	0.167	199.9	0.70	1, 3, 8, 15, 25, 63
SV2	90	Pure water	0.884	100.2	7.4	1, 3, 8, 15, 25, 63
PW-50-t1	50	Pure water	0.047	50.9	0.78	0.25
PW-50-t2	50	Pure water	0.041	50.2	0.69	0.29
PW-50-t3	50	Pure water	0.042	50.4	0.70	0.38
PW-50-t4	50	Pure water	0.043	51.6	0.70	0.67
PW-50-t5	50	Pure water	0.042	50.0	0.71	1.1
PW-50-t6	50	Pure water	0.042	51.7	0.68	2.0

* BG is basaltic glass

** S/V is the ratio of the basaltic glass reactive surface area (measured by BET) to the volume of solution used in the experiment

Table 2. $\delta^7\text{Li}$ (‰) obtained for several reference materials during sessions (1) and (2) using the Neptune MC-ICP-MS and the Nu Instruments MC-ICP-MS

Standard name		$\delta^7\text{Li}$ (‰)	$\delta^7\text{Li}$ (‰) published values
<i>Neptune (BRGM)</i>			
SW BCR-403 30 ppb		$+31.3 \pm 0.4$ (n=10)	$+31.0 \pm 0.1$ Millot et al. (2004)
Li7-N 30 ppb		$+30.8 \pm 0.5$ ‰ (n = 10)	$+30.2 \pm 0.3$ Carignan et al. (2007)
Li7-N* 30 ppb		$+30.3 \pm 0.2$ ‰ (n = 10)	
Li6-N* 30 ppb		-8.1 ± 0.2 ‰ (n = 10)	-8.0 ± 0.3 Carignan et al. (2007)
<i>Nu Instruments (ENS)</i>			
Basalt JB-2	(1)	$+4.0 \pm 0.3$ (n = 1)	$+4.6 \pm 0.9$ Carignan et al. (2007)
SW BCR-403	(1)	$+30.9 \pm 0.2$ (n = 1)	$+31.3 \pm 0.6$ Millot et al. (2004)
SW BCR-403 30-60 ppb	(2)	$+30.8 \pm 0.6$ (n = 3)	
SW BCR-403 15 ppb	(2)	$+30.5 \pm 0.7$ (n = 2)	
Li7-N (50-100 ppb)*	(1)	$+30.2 \pm 0.3$ ‰ (n = 4)	$+30.2 \pm 0.3$ Carignan et al. (2007)
Li7-N (25 ppb)*	(1)	$+30.0 \pm 0.4$ ‰ (n = 2)	
Li7-N (50-75 ppb)*	(2)	$+30.0 \pm 0.4$ ‰ (n = 14)	
Li7-N (10 to 40 ppb)*	(2)	$+29.9 \pm 0.6$ ‰ (n = 11)	
Li6-N (25-50 ppb)*	(1)	-8.1 ± 0.4 ‰ (n = 3)	-8.0 ± 0.3 Carignan et al. (2007)
Li6-N (50 ppb)*	(2)	-8.1 ± 0.4 ‰ (n = 7)	

Uncertainties are given at the 2σ level. See text for more details.

* These standards were not passed through the chemical separation procedure

Table 3. Composition of the Li-enriched synthetic basaltic glass (VBS) used in all of the experiments

Oxide Wt. %	VBS
SiO₂	49.08
Al₂O₃	14.78
Fe₂O₃	10.82
MnO	0.21
MgO	8.18
CaO	10.69
Na₂O	2.69
K₂O	0.18
TiO₂	1.73
P₂O₅	0.13
Li₂O	0.964
Total	99.46

ACCEPTED MANUSCRIPT

Table 4. pH, elemental concentrations and $\delta^7\text{Li}$ (‰) of the solutions recovered from alteration experiments. pH is given at the temperature of the experiment (90°C for all experiments, except PW-50 at 50°C). LD (limit of detection) are 1 ppm for Al, 0.02 ppm for Fe, 0.1 ppm for Mg. Leachates were diluted by a factor 2 in the experiments PH3-90 and PH10-90 and by a factor 5 for the experiments SV1 and SV2. Si/Li is in ppm/ppm. Uncertainties for $\delta^7\text{Li}$ are given at the 2σ level and correspond to the internal error.

Exp.	S/V cm ⁻¹	Time d	pH	Si ppm	Al ppm	Fe ppm	Mg ppm	Ca ppm	Na ppm	Li ppm	Si/Li	$\delta^7\text{Li}$ ‰
PW-90	0.70	0.02	7.9	0.19	< LD	< LD	< LD	0.28	0.30	0.020	9.5	+4.9 ± 0.2
	0.71	0.42	8.6	6.60	2.66	< LD	1.62	2.28	-	0.136	48.5	+9.3 ± 0.5
	0.72	0.58	8.6	8.80	3.57	< LD	< LD	2.94	0.95	0.170	51.8	+10.0 ± 0.4
	0.71	0.79	8.6	8.76	3.55	< LD	1.82	2.99	0.92	0.199	44.0	+10.3 ± 0.3
	0.71	3.8	8.6	13.1	4.01	< LD	< LD	5.11	2.02	0.434	30.2	+10.0 ± 0.3
PH3-90	0.71	0.08	3.0	1.28	< LD	0.570	< LD	0.870	0.256	0.065	19.7	nd
	0.72	0.21	3.1	2.30	< LD	0.661	< LD	1.15	0.336	0.095	24.2	+9.7 ± 1.1
	0.74	0.33	3.1	3.15	< LD	0.630	< LD	1.43	0.374	0.106	29.7	nd
	0.76	1.0	3.1	5.08	2.23	0.784	1.18	2.05	0.584	0.145	35.0	+8.8 ± 1.6
	0.78	1.3	3.3	5.56	2.38	0.798	1.24	2.05	0.587	0.163	34.1	nd
	0.80	2.0	3.4	6.63	2.79	0.884	1.51	2.42	0.677	0.175	37.9	+9.7 ± 0.8
	0.82	34.3	4.2	17.8	< LD	1.75	4.67	6.89	1.93	0.394	45.2	+9.6 ± 0.2
PH10-90	0.71	0.08	8.4	1.19	< LD	< LD	< LD	< LD	0.45	0.045	26.4	+9.5 ± 0.9
	0.73	0.21	8.4	3.06	< LD	< LD	< LD	0.784	0.64	0.092	33.3	+10.0 ± 1.3
	0.75	0.33	8.3	4.10	< LD	< LD	< LD	1.326	0.75	0.121	33.9	nd
	0.76	1.0	8.3	7.90	3.19	< LD	1.74	2.78	1.25	0.207	38.2	+10.1 ± 0.6
	0.79	1.3	8.2	8.74	3.53	< LD	1.88	2.80	1.21	0.249	35.1	nd
	0.81	2.0	8.2	10.3	4.15	< LD	2.20	3.37	1.49	0.299	34.4	+10.1 ± 1.0
	0.84	34.3	8.2	14.2	< LD	< LD	< LD	5.58	3.11	0.591	24.0	+10.5 ± 0.2
SV1	0.70	1.0	8.1	5.59	< LD	< LD	< LD	< LD	0.91	0.138	40.5	+10.0 ± 0.2
	0.73	3.3	8.7	9.76	< LD	< LD	< LD	3.36	1.25	0.259	37.7	+10.3 ± 0.2
	0.75	8.3	8.8	11.4	< LD	< LD	< LD	4.16	1.80	0.395	28.9	+10.2 ± 0.2
	0.77	15.2	8.5	12.7	< LD	< LD	< LD	-	2.61	0.491	25.9	+10.4 ± 0.2
	0.80	25.1	8.8	13.9	< LD	< LD	< LD	4.05	2.08	0.494	28.1	+10.4 ± 0.2
	0.81	63.3	8.9	14.8	< LD	< LD	< LD	4.96	3.49	0.674	22.0	nd
SV2	7.4	1.0	8.8	11.4	< LD	< LD	< LD	4.88	1.78	0.413	27.6	+8.6 ± 0.2
	7.5	3.3	8.5	12.6	< LD	< LD	< LD	< LD	2.30	0.595	21.2	+8.8 ± 0.2
	7.7	8.3	8.9	13.2	< LD	< LD	< LD	4.92	3.00	0.746	17.7	nd
	7.8	15.2	9.0	14.1	< LD	< LD	< LD	5.08	3.75	0.872	16.2	+8.9 ± 0.2
	7.9	25.1	9.0	16.1	< LD	< LD	< LD	6.01	3.96	0.918	17.5	+9.0 ± 0.2
	8.0	63.3	9.1	15.1	< LD	< LD	< LD	6.40	4.76	1.309	11.5	+8.9 ± 0.6
	PW-50	0.78	0.25	6.6	0.031	< LD	< LD	-				
0.69		0.29	6.6	0.034	< LD	-	+5.9 ± 0.7					
0.70		0.39	6.6	0.064	< LD	-	+6.6 ± 0.7					
0.70		0.71	7.6	0.065	< LD	0.013	5.0	+6.5 ± 0.4				
0.71		1.1	7.7	0.139	< LD	0.021	6.6	+6.7 ± 0.4				
0.68		2.0	7.7	0.177	< LD	0.021	8.4	+7.5 ± 0.4				

Table 5. Normalized mass losses of elements from the glass (Eq. (2)). Relative uncertainties are 10%.

Exp.	Time days	NL(Si) g·m ⁻²	NL(Al) g·m ⁻²	NL(Fe) g·m ⁻²	NL(Mg) g·m ⁻²	NL(Ca) g·m ⁻²	NL(Na) g·m ⁻²	NL(Li) g·m ⁻²
PW-90	0.01	0.012				0.052	0.215	0.064
	0.43	0.405	0.479		0.462	0.420		0.428
	0.58	0.533	0.634			0.534	0.661	0.527
	0.79	0.538	0.639		0.520	0.551	0.649	0.626
	3.8	0.804	0.722			0.942	1.426	1.365
PH3-90	0.08	0.079		0.106		0.160	0.181	0.204
	0.21	0.139		0.121		0.209	0.234	0.295
	0.33	0.186		0.112		0.253	0.253	0.320
	1.0	0.291	0.375	0.136	0.315	0.353	0.385	0.426
	1.3	0.311	0.390	0.135	0.322	0.344	0.377	0.467
	2.0	0.361	0.446	0.146	0.383	0.396	0.424	0.488
	34.3	0.946		0.282	1.154	1.100	1.179	1.073
PH10-90	0.08	0.073					0.318	0.141
	0.21	0.183				0.141	0.439	0.281
	0.33	0.238				0.231	0.501	0.360
	1.0	0.453	0.537		0.464	0.479	0.824	0.608
	1.3	0.482	0.571		0.482	0.464	0.768	0.704
	2.0	0.554	0.655		0.551	0.545	0.922	0.824
	34.3	0.737				0.869	1.855	1.571
SV1	1.0	0.348					0.651	0.440
	3.3	0.583				0.602	0.858	0.792
	8.3	0.663				0.726	1.203	1.176
	15.2	0.719					1.699	1.423
	25.1	0.757				0.663	1.303	1.378
	63.3	0.798				0.804	2.164	1.862
SV2	1.0	0.067				0.086	0.121	0.125
	3.3	0.073					0.154	0.177
	8.3	0.075				0.084	0.195	0.216
	15.2	0.079				0.085	0.241	0.250
	25.1	0.089				0.100	0.251	0.259
	63.3	0.082				0.105	0.298	0.378
PW-50	0.24	0.002						
	0.29	0.002						
	0.39	0.004						
	0.69	0.004						0.041
	1.09	0.009						0.066
	2.04	0.011						0.069

Table 6. Parameters and results of the model. The parameters τ and r_0 are used to fit the dissolution rate r (Eq. (10)). D is the 'true' Li diffusion coefficient used in the model. The ratio a is the D_7/D_6 ratio, and n is the number of data points used for the modelling. The range of uncertainties for a considers all of the measured $\delta^7\text{Li}$ values. The corresponding β values (see Eq. (6)) are also shown.

Exp.	Time	τ (d)	r_0 (g/m ² /d)	D (m ² /d)	a	β
PW90	$t \leq 4$ d	0.919	0.930	$2.6 \cdot 10^{-14}$	0.990 (n=5) 0.997 (n=4)	0.078 0.019
PH3-90	$t \leq 2$ d	0.419	0.812	$0.9 \cdot 10^{-14}$	0.994 ± 0.004 (n=3)	0.039
PH10-90	$t \leq 2$ d	0.589	0.949	$1.9 \cdot 10^{-14}$	0.997 ± 0.002 (n=4)	0.019
SV1	$t \leq 15$ d	1.533	0.448	$1.7 \cdot 10^{-12}$	1.000 ± 0.002 (n=4)	0
SV2	$t \leq 15$ d	0.464	0.163	$6.0 \cdot 10^{-14}$	0.997 ± 0.002 (n=3)	0.019
PW50	$t \leq 2$ d	1.701	0.010	$4.0 \cdot 10^{-16}$	0.991 ± 0.003 (n=6)	0.059

ACCEPTED MANUSCRIPT